
SPATIAL MODEL CHECKING OF IMAGES VIA MINIMISED MODELS AND BRANCHING BISIMILARITY

VINCENZO CIANCIA ^a, JAN FRISO GROOTE ^b, DIEGO LATELLA ^c, MIEKE MASSINK ^a,
AND ERIK P. DE VINK ^b

^a Istituto di Scienza e Tecnologie dell’Informazione “A. Faedo”, Consiglio Nazionale delle Ricerche,
Pisa, Italy
e-mail address: Vincenzo.Ciancia@cnr.it, Mieke.Massink@cnr.it

^b Eindhoven University of Technology, Eindhoven, the Netherlands
e-mail address: J.F.Groote@tue.nl, E.P.d.Vink@tue.nl

^c Formerly with Istituto di Scienza e Tecnologie dell’Informazione “A. Faedo”, Consiglio Nazionale
delle Ricerche, Pisa, Italy. Retired
e-mail address: diego.latella@actiones.eu

ABSTRACT. Spatial models are of increasing interest in traditional computer science domains and beyond. Spatial minimisation procedures are crucial for efficient model checking of such models that are often large in size. For the recent notion of spatial bisimilarity for quasi-discrete closure models, called “Compatible Paths” (CoPa) bisimilarity, an effective minimisation method is proposed, and shown to be correct. Reasoning about space represented by quasi-discrete closure models involves two different conditional reachability modalities: a forward reachability, similar to that used in temporal logic, and a backward modality, representing the fact that a point can be reached from another point, under certain conditions. The core of our minimisation method is the encoding of closure models as labelled transition systems, enabling minimisation algorithms for branching bisimilarity to compute CoPa equivalence classes. A prototype toolchain, **VoxMinX**, is proposed to validate the minimisation method. **VoxMinX** preserves the relationship between equivalence classes and sets of pixels in the original image. Experimental validation of the toolchain via benchmark examples demonstrates a promising speed-up in model checking of spatial properties for models of realistic size.

Key words and phrases: Closure Spaces; Spatial Logics; Spatial Bisimilarity; Branching Bisimilarity; Spatial Model Checking; Minimal Model.

* Research partially funded by the Italian MUR Projects PRIN 2017FTXR7S, “IT- MaTTerS”, PRIN 2020TL3X8X “T-LADIES”, and Next Generation EU - MUR Project PNRR PRI ECS00000017 “THE - Tuscany Health Ecosystem”.

The authors are listed in alphabetical order as they equally contributed to the work presented in this paper. The present paper has been produced without the help of any AI system.

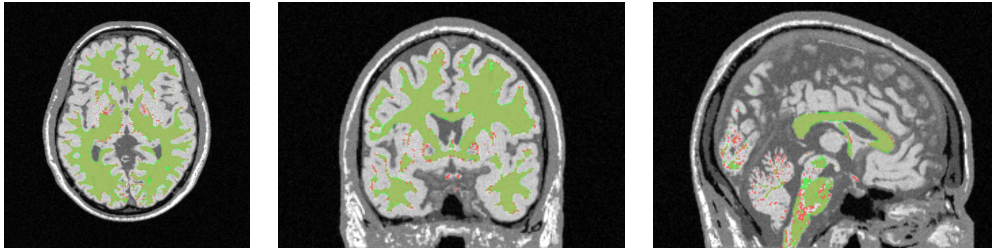


FIGURE 1. Cross section of a dataset element of BrainWeb [ABGP⁺06] pat04 MRI at slice $(x, y, z) = (129, 147, 78)$, (axial view left, coronal view middle, sagittal view right): VoxLogicA analysis of the segmentation of white matter, shown as a green overlay on top of a red overlay representing the ground truth.

1. INTRODUCTION

Spatial model checking consists in the automatic verification of properties, expressed in a suitable spatial logic, on each point of a suitable spatial model. In [CLLM14] the Spatial Logic for Closure Spaces (SLCS) was introduced and further developed in [CLLM16]. Closure spaces, or Čech closure spaces [Č66], are a generalisation of topological spaces suitable to model many kinds of spatial objects, ranging from topological objects in continuous spaces, such as Euclidean spaces, to discrete spatial objects, such as general and regular graphs. The latter are particularly useful to represent digital images. Closure spaces (CS) and the sub-class of quasi-discrete closure spaces, QdCSs for short, form a convenient theoretical framework because of their generality and relative simplicity. A practical demonstration of this is the tool VoxLogicA, a recently developed spatial model checker that can efficiently check SLCS properties of large digital images represented as *symmetric* quasi-discrete closure models—QdCMs, i.e. models with QdCSs as underlying spaces [BCLM19b, BCLM19a, BBC⁺21].

Spatial and spatio-temporal model checking have been successfully employed, in the past years, in a variety of application areas, ranging from Collective Adaptive Systems [CLM⁺16, CGG⁺18] to signals [NBC⁺18], images [CLLM16, HJK⁺15, BBC⁺20] and polyhedra [BCG⁺22], just to mention a few. These methods for spatial analysis are enjoying an increasing interest in computer science and beyond, also in unexpected domains such as medical imaging [BCLM19b, BBC⁺21]. Medical images are obtained from diagnostic instruments such as magnetic resonance images (MRI), computer tomography scans, positron emission tomography, or dermoscopic images. Such images usually consist of millions of pixels, in 2D, or voxels (volumetric pixels) in 3D images.

For example, in our earlier work [BCLM19a], the 3D MRI image of a healthy brain shown in Figure 1 consists of circa 12M voxels (i.e. $256 \times 256 \times 181$) requiring approximately 10 seconds to analyse using VoxLogicA on a desktop computer.¹ VoxLogicA checks a logical specification for *every* point in the model exploiting parallel execution, memoization, and state-of-the-art imaging libraries [BCLM19b]. VoxLogicA internally creates a QdCM of the

¹In that work we used an Intel Core I9 9900K processor (with 8 cores) and 32GB of RAM.

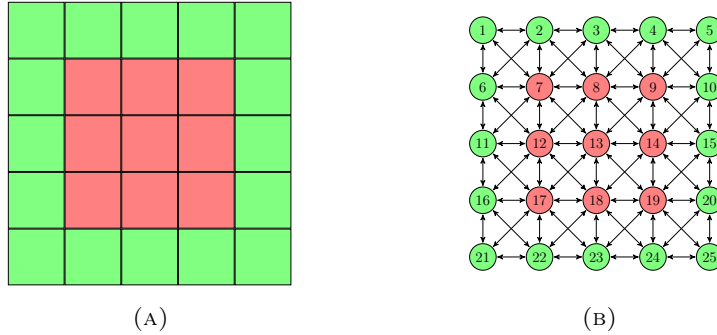


FIGURE 2. Figure 2a: A pixel based image with green and red pixels. Figure 2b: A finite, symmetric QdCM in the shape of a regular graph with nodes representing pixels and edges representing the 8-adjacency relation between the pixels of the image in Figure 2a.

pixel-based, or voxel-based, image that it is given as input. Such models take the form of a symmetric regular 8-adjacency graph, in which nodes are representing pixels (voxels) and edges between nodes are representing the adjacency between pixels represented by the nodes. Both adjacency in north-south direction and in east-west direction are considered, as well as diagonal adjacency. Figure 2a shows a simple pixel-based image and Figure 2b its related QdCM (except for the self-loops, that have been omitted to avoid clutter in the figure).

A detailed description of `VoxLogicA`, its application to the contouring of high grade glioblastoma, a malignant type of brain tumour tissue, and to the identification of grey and white matter in the brain can be found in [BCM25]. In the same work also a hybrid contouring method has been proposed, combining the symbolic spatial model checking method with `nnU-Net` [IJK⁺21, IWU⁺24], a sub-symbolic deep learning method. Such a hybrid approach may provide a human explainable method for the contouring while gaining in precision enhancing the results with the deep learning approach.

A way to increase the time and space efficiency of spatial model checking is to exploit suitable model minimisation algorithms based on *spatial* bisimilarity. For that purpose several spatial bisimilarities have been proposed in [CLMV22, CLMV25]. In particular, CoPa-bisimilarity, based on a notion of “path-compatibility” is promising. The notion of path compatibility essentially requires that two paths, in order to be compatible, have to be both composed of a (non-empty) sequence of an equal number of non-empty adjacent “zones”, such that each point in one zone of one path must be related, by the bisimulation relation, to every point in the corresponding zone of the other path (see the illustration in Figure 4b).

In [CLMV22, CLMV25], a logical characterisation of CoPa-bisimilarity has been given. More precisely, Infinitary Compatible Reachability Logic (ICRL) has been defined that is a modal logic with infinitary conjunction and two modalities, $\vec{\zeta}$ and $\overleftarrow{\zeta}$, expressing conditional forward and backward reachability, respectively. Given two ICRL formulas Φ_1 and Φ_2 , a point x satisfies $\vec{\zeta}\Phi_1[\Phi_2]$ if x satisfies Φ_1 , or x satisfies Φ_2 and there is a path from x to a

point y satisfying Φ_1 where all the points on the path between x and y satisfy Φ_2 . Similarly for $\zeta\Phi_1[\Phi_2]$, which is satisfied by x if x satisfies Φ_1 , or x satisfies Φ_2 and there is a path from a point y satisfying Φ_1 , to x , where all the points on the path between y and x satisfy Φ_2 .²

Building on our previous work [CGL⁺23b], this paper includes two original contributions, one of a more theoretical nature and the other more practical in kind.

Theoretical contribution. The paper introduces an encoding of finite Closure Models (CMs), a sub-class of QdCMs, into Labelled Transition Systems (LTS) that preserves CoPa-bisimilarity. More precisely, two points in the input CM are CoPa-bisimilar if and only if the states they are mapped to by the encoding are branching bisimilar [GW96, GJKW17, JGKW20, GJ25]. Thus, given a finite CM, the encoding makes it possible to effectively compute the minimal model with respect to CoPa-bisimilarity via the composition of the encoding and a very efficient minimisation algorithm for branching bisimilarity, proposed in [GJKW17, JGKW20, GJ25] and implemented as part of the mCRL2 tool set [BGK⁺19]. In addition, detailed correctness proofs, including those concerning the encoding, are provided.

Practical contribution. To validate the approach, we apply it to digital images, which are a special case of (symmetric) finite closure models. A digital image is usually composed of a large number of pixels (i.e. points in the closure space representing the image) and, therefore, digital images represent an interesting benchmark for the minimisation procedure. In particular, a prototype experimental implementation of the encoding has been developed which, in turn, is part of a more complex toolchain, **VoxMinX**, used for the analysis of digital images. The toolchain comprises the implementation of the encoding developed in the theoretical part and produces a minimal model, exploiting the branching bisimulation minimisation procedure provided by the tool set mCRL2 [BGK⁺19]. The resulting minimal model is suitable for model checking with **GraphLogicA**, a spatial model checker for the finitary version of ICRL, that takes decorated graphs as input, representing general finite closure models. The minimal model produced by **VoxMinX** maintains the relationship between the equivalence classes, that are represented by states of the minimal model, and the respective sets of pixels of the original digital image. In this way, the spatial model checking results can directly be visualised on the original image, for example by highlighting the pixels that satisfy a spatial property of interest. **VoxMinX** extends the preliminary toolchain that was introduced in our previous work [CGL⁺23b]. The **VoxMinX** toolchain is evaluated on a benchmark of images at various resolutions. In this evaluation the model checking performance of **VoxMinX** is compared to that of **VoxLogicA**, since **VoxLogicA** is an optimised spatial model checker for non-minimised digital images, and therefore it forms a state-of-the-art basis for comparison. The evaluation shows that a considerable speed-up can be obtained in model checking time, especially when comparing the times for larger images, suggesting interesting directions for future research and applications.

²Note that, different from the context of classical temporal logics, in the context of space, and in particular when dealing with notions of directionality (e.g. one way roads, public area gates), it is important to be able to distinguish between the concept of “reaching” and that of “being reached”. The interested reader is referred to [CLMV22, CLMV25] for a discussion on the issue.

Related work. Qualitative reasoning about spatial entities [CR08] has been, and still is, a very active area of research in which the theory of topology and closure spaces play a important role. Prominent examples of that area are the region connection calculi, such as RCC8D. An embedding of the latter in the collective variant of SLCS was presented in [CLM19]. Our work is mainly inspired by spatial logics (see [APB07] for an extensive overview), with seminal work dating back to Tarski and McKinsey in the forties of the previous century. The work on *spatial model checking* for logics with reachability originated in [CLLM16], which includes a comparison to the work of Aiello on spatial *until* operators (see e.g. [Aie02]). In [Aie03], Aiello envisaged practical applications of topological logics with *until* to minimisation of images. The present paper builds on and extends that vision. Bisimilarity for spatial logics with reachability is a relatively new subject. In [LPS20], a bisimulation relation that is correct with respect to SLCS has been presented. Such a definition has not yet been proved complete and is aimed at characterising the logic including the *near* operator, therefore, not quotienting up-to reachability, as done in the present paper. The work in [BCG⁺22, CGL⁺23a, BCG⁺24] and that in [LQ23] introduce bisimulation relations that characterise spatial logics with reachability in polyhedral models and in simplicial complexes, respectively. It will be interesting future work to apply the minimisation techniques we present also to such relevant classes of models. First results in that direction can be found in [BBC⁺26] where weak simplicial bisimilarity and related minimisation procedures are presented for use in polyhedral model checking.

In the Computer Science literature, other kinds of spatial logics have been proposed that typically describe situations in which modal operators are interpreted *syntactically* against the structure of agents in a process calculus. We refer to [CG00, CC03] for some classical examples. Along the same lines, a recent example is given in [TPGN15], concerning model checking of security aspects in cyber-physical systems, in a spatial context based on the idea of bigraphical reactive systems introduced by Milner [Mil09]. A bigraph consists of two graphs: A place graph, i.e. a forest defined over a set of nodes which is intended to represent entities and their locality in terms of a containment structure, and a link graph, a hypergraph composed over the same set of nodes representing arbitrary linking among those entities. The QdCS models that are the topic of the present paper, instead, address space from a topological point of view rather than as a containment structure for spatial entities.

There is also active research on the improvement of the performance of branching bisimilarity minimisation algorithms. A recent contribution can be found in [JK26].

The structure of the paper is as follows. Section 2 recalls relevant concepts and introduces notation. Section 3 recalls CoPa-bisimilarity for QdCMs. In Section 4 the encoding of finite QdCMs into LTSs is presented, together with the correctness results. Section 5 describes a feasibility study and experimental evaluation of **VoxMinX** applying it to three families of representative benchmark examples. Appendix A shows a small running example for the transformations and minimisation performed by the **VoxMinX** toolchain.

2. PRELIMINARIES

We first introduce some relevant concepts and notation, in particular recalling LTSs, branching bisimilarity [GW96, GJKW17, JGKW20], (quasi-discrete) closure spaces, and closure models and paths therein.

Given a set X , $\mathcal{P}(X)$ denotes the powerset of X . The set of natural numbers is denoted by \mathbb{N} . For $n, m \in \mathbb{N}$ we often use the interval notation $[m, n]$ denoting the set

$\{i \in \mathbb{N} \mid m \leq i \leq n\}$, $[m, n)$ denoting the set $\{i \in \mathbb{N} \mid m \leq i < n\}$, and similarly for $(m, n]$ and (m, n) .

In the sequel, branching bisimilarity [GW96, GJKW17, JGKW20] of states of LTSs plays a central role. Below we recall the relevant definitions.

Definition 2.1 (Labelled Transition System - LTS). A *Labelled Transition System*, LTS for short, is a tuple $(S, \mathcal{A}, \rightarrow)$ where S and \mathcal{A} are non-empty sets of *states*, and *actions*, respectively, and relation $\rightarrow \subseteq S \times \mathcal{A} \times S$ is the *transition relation*.

As usual, we distinguish an action $\tau \in \mathcal{A}$ that models a “silent move” in the LTS. Moreover, we call the elements of the relation \rightarrow *transitions*, and we write $s \xrightarrow{\alpha} s'$ whenever $(s, \alpha, s') \in \rightarrow$. A *computation* in the LTS is an alternating sequence $s_0 \xrightarrow{\alpha_1} s_1 \cdots s_{n-1} \xrightarrow{\alpha_n} s_n$ of states and actions where $n \geq 0$ and $s_{i-1} \xrightarrow{\alpha_i} s_i$ for $i = 1, \dots, n$. We have occasion to write $s \xrightarrow{\tau}^* s'$ if with respect to the above situation we have $s = s_0$, $\alpha_i = \tau$ for $i = 1, \dots, n$, and $s' = s_n$.

Definition 2.2 (Branching bisimilarity – \leftrightarrow_b). Given an LTS $\mathcal{S} = (S, \mathcal{A}, \rightarrow)$, a symmetric relation $B \subseteq S \times S$ is a *branching bisimulation for \mathcal{S}* iff, for $s, t, s' \in S$ and $\alpha \in \mathcal{A}$, whenever sBt and $s \xrightarrow{\alpha} s'$, it holds that

- (i) $s'Bt$ and $\alpha = \tau$, or
- (ii) $sB\bar{t}$, $s'Bt'$ and $t \xrightarrow{\tau}^* \bar{t}$, $\bar{t} \xrightarrow{\alpha} t'$ for some $\bar{t}, t' \in S$

Two states $s, t \in S$ are called *branching bisimilar* in \mathcal{S} if sBt for some branching bisimulation B for \mathcal{S} . Notation, $s \leftrightarrow_b^{\mathcal{S}} t$.

From now on, for readability, we omit the superscript \mathcal{S} in $\leftrightarrow_b^{\mathcal{S}}$, when this does not cause confusion.

Our framework for modelling space is based on the notion of a *Čech closure space* [Č66], CS for short, that provides a convenient common framework for the study of several different kinds of spatial models, including models of both discrete and continuous space [SW07]. We briefly recall definitions and results on CSs, that are relevant for this paper — most of which are borrowed from [Gal03] (see also [CLMV22, CLMV25, CLLM16]).

Definition 2.3 (Closure Space – CS). A *closure space* is a pair (X, \mathcal{C}) where X is a set (of *points*) and $\mathcal{C} : \mathcal{P}(X) \rightarrow \mathcal{P}(X)$ is the *closure operator*, i.e., a function satisfying the following axioms:

- (i) $\mathcal{C}(\emptyset) = \emptyset$,
- (ii) $A \subseteq \mathcal{C}(A)$ for all $A \subseteq X$, and
- (iii) $\mathcal{C}(A_1 \cup A_2) = \mathcal{C}(A_1) \cup \mathcal{C}(A_2)$ for all $A_1, A_2 \subseteq X$.

It is worth pointing out that CSs are a generalisation of topological spaces. In fact, the latter coincide with CSs that satisfy the *idempotence* axiom, i.e., $\mathcal{C}(\mathcal{C}(A)) = \mathcal{C}(A)$ for all $A \subseteq X$.

Definition 2.4 (Quasi-discrete closure space – QdCS). A *quasi-discrete closure space* is a CS (X, \mathcal{C}) such that for each $A \subseteq X$ it holds that $\mathcal{C}(A) = \bigcup_{x \in A} \mathcal{C}(\{x\})$.

Thus, the closure operator in a QdCS is determined by its value for the singleton. For brevity, we have occasion to write $\mathcal{C}(x)$ instead of $\mathcal{C}(\{x\})$.

Given a relation $R \subseteq X \times X$, define the function $\mathcal{C}_R : \mathcal{P}(X) \rightarrow \mathcal{P}(X)$ as follows: for all $A \subseteq X$, we put $\mathcal{C}_R(A) = A \cup \{x \in X \mid \exists a \in A : aRx\}$. It is easy to see that, for any R ,



FIGURE 3. Figure 3a: A finite QdCS (X, \mathcal{C}_R) . The arrows represent the relation R underlying \mathcal{C}_R . The points of the set $A \subseteq X$ are shown in white, remaining points are shown in black. Figure 3b: Points in $\mathcal{C}_R(A) \setminus A$ are shown in grey.

\mathcal{C}_R satisfies all the axioms of Definition 2.3 and so (X, \mathcal{C}_R) is a CS. An example of the result of applying the closure operator \mathcal{C}_R induced by a relation R to a set A is shown in Figure 3.

The following theorem is a standard result in the theory of CSs [Gal03].

Theorem 2.5. *A CS (X, \mathcal{C}) is quasi-discrete if and only if there is a relation $R \subseteq X \times X$ such that $\mathcal{C} = \mathcal{C}_R$. \square*

The above theorem implies that any graph coincides with a QdCS where the relation underlying the closure operator is exactly the edge relation of the graph. We prefer to treat graphs as QdCSs since in this way we can formulate key definitions at the level of closure spaces leading to a uniform treatment for graphs and other kinds of models for space (e.g. topological spaces) [SW07]. Furthermore, if X is finite, any closure space (X, \mathcal{C}) is quasi-discrete: For $A \subseteq X$ it holds that

$$\mathcal{C}(A) = \mathcal{C}(\bigcup\{\{x\} \mid x \in A\}) = \bigcup\{\mathcal{C}(\{x\}) \mid x \in A\}$$

by axiom (iii) of Definition 2.3 and finiteness of A . In the sequel, we consider only *finite* CSs, hence only QdCSs. and often refrain from explicitly writing the subscript R in \mathcal{C}_R , when this does not cause confusion. Finally, we say that (X, \mathcal{C}) is a *symmetric* QdCS if $\mathcal{C} = \mathcal{C}_R$ for a symmetric relation R . In such a case, it holds that $y \in \mathcal{C}(\{x\}) \Leftrightarrow x \in \mathcal{C}(\{y\})$ for $x, y \in X$.

In the context of the present paper, *paths* over CSs play an important role. Following the tradition in topology, in the theory of CSs paths are defined as continuous functions from an appropriate index space to the CS at hand. For finite CSs, it is sufficient to consider finite paths.

Definition 2.6 (Finite path). A (finite) path in a CS (X, \mathcal{C}) is a function $\pi : [0, \ell] \rightarrow X$, for some $\ell \in \mathbb{N}$, such that $\pi(i+1) \in \mathcal{C}(\{\pi(i)\})$ for $i = 0, \dots, \ell-1$. We call ℓ the *length* of π and we denote it by $\text{len}(\pi)$.

In the sequel, we will say that a path $\pi : [0, \ell] \rightarrow X$ in a finite CS (X, \mathcal{C}) is a *path from* $x \in X$ if $\pi(0) = x$ and it is a *path to* x if $\pi(\ell) = x$. Furthermore, we will use the notation $(x_i)_{i=0}^\ell$ for the path $\pi : [0, \ell] \rightarrow X$ such that $\pi(i) = x_i$ for all $i \in [0, \ell]$.

Remark 2.7. It is worth pointing out that the notion of path in a QdCS is similar to that of a path in a graph or of a computation in an LTS, but it is *not* the same. In particular,

due to axiom (ii) of closure operator \mathcal{C} and the requirement $\pi(i+1) \in \mathcal{C}(\pi(i))$, paths in CSs allow *stuttering*; in other words, for QdCS (X, \mathcal{C}) , $x \in X$, and path π , it may happen that $\pi(i) = \pi(i+1) = x$, for $i < \pi(\text{len}(\pi))$ *even when* (x, x) is *not* an element of the relation $R \subseteq X \times X$ underlying \mathcal{C} . This is different for a path $\dots n_1 n_2 \dots$ in a graph (N, E) , where in order for nodes n_1 and n_2 in N to be adjacent, it is required that (n_1, n_2) is an element of the edge relation E . A similar issue arises when comparing paths in QdCSs with traces in LTSs. In fact, for LTS $(S, \mathcal{A}, \rightarrow)$, two states s_1 and s_2 can be adjacent in a computation $\dots s_1 \xrightarrow{\alpha} s_2 \dots$ *only* if $(s_1, \alpha, s_2) \in \rightarrow$, and this holds also if $s_2 = s_1$.

We assume a set AP of *atomic proposition letters* is given and introduce the notion of *closure model* (CM for short).

Definition 2.8 (Closure model – CM). A *closure model* is a tuple $\mathcal{M} = (X, \mathcal{C}, \mathcal{V})$, with (X, \mathcal{C}) a CS, and $\mathcal{V} : \text{AP} \rightarrow \mathcal{P}(X)$ the *valuation function*, assigning to each $p \in \text{AP}$ the set of points where p holds.

All definitions for CSs also apply to CMs; thus, a *quasi-discrete closure model* (QdCM for short) is a CM $\mathcal{M} = (X, \mathcal{C}, \mathcal{V})$ where (X, \mathcal{C}) is a QdCS. Similarly, a *symmetric QdCM* is a QdCM $(X, \mathcal{C}, \mathcal{V})$ where (X, \mathcal{C}) is a symmetric QdCS. For a closure model $\mathcal{M} = (X, \mathcal{C}, \mathcal{V})$ we may write $x \in \mathcal{M}$ when $x \in X$. Similarly, we speak of paths in \mathcal{M} meaning paths in (X, \mathcal{C}) . Finally, with respect to \mathcal{M} , for $x, y \in X$, we have $x =_{\mathcal{V}} y$ if $x \in \mathcal{V}(p) \Leftrightarrow y \in \mathcal{V}(p)$ for all $p \in \text{AP}$, and $x \neq_{\mathcal{V}} y$ if not $x =_{\mathcal{V}} y$.

In the sequel, for a logic \mathcal{L} , a formula $\Phi \in \mathcal{L}$, and a model $\mathcal{M} = (X, \mathcal{C}, \mathcal{V})$ we let $[[\Phi]]_{\mathcal{L}}^{\mathcal{M}}$ denote the set $\{x \in X \mid \mathcal{M}, x \models_{\mathcal{L}} \Phi\}$ of all the points in \mathcal{M} that satisfy Φ , where $\models_{\mathcal{L}}$ is the satisfaction relation for \mathcal{L} . For the sake of readability, we refrain from writing the subscript \mathcal{L} when this does not cause confusion.

3. CoPA-BISIMILARITY FOR QDCM

In [CLMV22, CLMV25] several notions of spatial bisimilarity for closure models have been investigated. In particular, CM-bisimilarity, and its refinement for QdCMs CMC-bisimilarity, are a fundamental starting point for the study of spatial bisimilarity because of their strong links to topo-bisimilarity. However, CM and CMC are rather fine-grained relations for reasoning about general properties of space, since they are directly based on the closure operator.³ For instance, with reference to the model of Figure 4a, where all black points satisfy only atomic proposition b while the grey ones satisfy only g , the point at the center of the model is *not* CMC-bisimilar to any other black point. This is because CMC-bisimilarity is based on the fact that points reachable “in one step” — i.e. contained in the closure — are taken into consideration. This, in turn, gives bisimilarity a flavour of “counting”, that goes against the idea that, for instance in Figure 4a, all black points in the model are to be considered spatially equivalent. In fact, they are all black and all can reach black or grey points. Furthermore, they could be considered equivalent to the black point of a smaller model consisting of just one black and one grey point mutually connected—that would, in

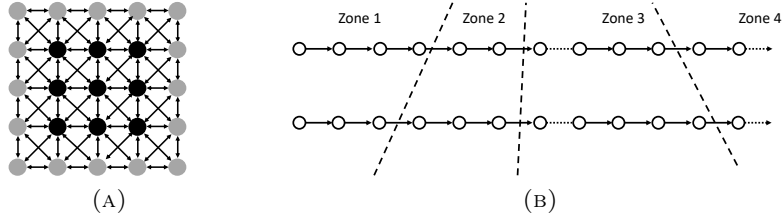


FIGURE 4. A model (a); zones in paths (b).

fact, be a “minimal” — in a sense that will be made clear later in the paper — representation of the closure model.

In order to relax the “counting” capability of CMC-bisimilarity for QdCSs as mentioned, a weaker notion of bisimilarity has been introduced in [CLMV22, CLMV25] that is based on paths, instead of membership of closures, together with a notion of “compatibility” between relevant paths that essentially requires each of them be composed of a non-empty sequence of non-empty, adjacent “zones”. More precisely, both paths under consideration in a transfer condition should share the same structure, as follows (see Figure 4b):

- both paths are composed by a sequence of (non-empty) “zones”;
- the number of zones should be the same in both paths, *but*
- the length of sub-path in “corresponding” zones can be different, *as well as* the length of each of the two paths;
- *each* point in a zone of a path should be related by the bisimulation to *every* point in the corresponding zone of the other path.

This notion of compatibility gives rise to the notion of *Compatible Path bisimulation*, more briefly CoPa-bisimulation, recalled below for QdCMs.

Definition 3.1 (path-compatibility). Given QdCM $\mathcal{M} = (X, \mathcal{C}, \mathcal{V})$ and relation $B \subseteq X \times X$, two paths $\pi = (x_i)_{i=0}^{\ell}$ and $\varrho = (y_j)_{j=0}^m$ in X are *compatible with respect to B* if $N > 0$ and two monotone surjections $f : [0, \ell] \rightarrow [1, N]$ and $g : [0, m] \rightarrow [1, N]$ exist such that $x_i B y_j$ for all indices $0 \leq i \leq \ell$ and $0 \leq j \leq m$ with $f(i) = g(j)$.

The functions f and g are referred to as *matching functions* for π and ϱ . The choice for N , f , and g is not unique. The minimal number $N > 0$ for which matching functions exist is defined to be the number of zones for the paths π and ϱ .

Definition 3.2 (CoPa-bisimilarity). A symmetric relation $B \subseteq X \times X$ is a *CoPa-bisimulation relation* for QdCS $\mathcal{M} = (X, \mathcal{C}, \mathcal{V})$ if, whenever $x, y \in X$ satisfy $x B y$, the following holds:

- (1) $x =_{\mathcal{V}} y$;
- (2) for every path π from x exists a B -compatible path ϱ from y ;
- (3) for every path π to x exists a B -compatible path ϱ to y .

Two points $x, y \in X$ are called *CoPa-bisimilar* in \mathcal{M} if $x B y$ for some CoPa-bisimulation relation B for \mathcal{M} . Notation, $x \rightleftharpoons_{\text{CoPa}} y$.

³Or its dual operator called ‘interior’.

For a model $\mathcal{M} = (X, \mathcal{C}, \mathcal{V})$, it is immediate from the definition that CoPa-bisimilarity $\equiv_{\text{CoPa}} \subseteq X \times X$ in \mathcal{M} , being the union of all CoPa-bisimulation relations, is a CoPa-bisimulation relation itself, actually the largest bisimulation relation. Moreover, as a consequence of Theorem 3.4 below, CoPa-bisimilarity \equiv_{CoPa} is an equivalence relation.

Lemma 3.3. *Let $\mathcal{M} = (X, \mathcal{C}, \mathcal{V})$ be a QdCM and let $B \subseteq X \times X$ be a symmetric relation such that for all $x, y \in X$ satisfying xBy it holds that*

- (1) $x =_{\mathcal{V}} y$;
- (2) if $x' \in \mathcal{C}(x)$ for some $x' \in X$, then a path $(y_j)_{j=0}^m$ from y exists for some $m \geq 0$ such that $y_j B x$ for all $j \in [0, m)$ and $y_m B x'$;
- (3) if $x \in \mathcal{C}(x')$ for some $x' \in X$, then a path $(y_j)_{j=0}^m$ to y exists for some $m \geq 0$ such that $y_j B x$ for all $j \in (0, m]$ and $y_0 B x'$;

Then B is a CoPa-bisimulation for \mathcal{M} .

Proof. We verify conditions (2) and (3) of Definition 3.2.

For the forward transfer condition (2), assume xBy and let $\pi = (x_i)_{i=0}^{\ell}$ be a path from x . We show by induction on ℓ that a B -compatible path ϱ from y exists. Basis, $\ell = 0$: The single point path $\varrho = (y)$ from y is B -compatible with π . Induction step, $\ell > 0$: Consider the path $\pi_0 = (x_0, x_1)$ of length 1 from x_0 and the path $\pi_1 = (x_i)_{i=1}^{\ell}$ of length $\ell - 1$ from x_1 . Because x_0By and $x_1 \in \mathcal{C}(x)$, by property (2) of B , a path $\varrho_0 = (y_j)_{j=0}^m$ from y for some $m \geq 0$ exists with $y_j B x_0$ for $j \in [0, m)$ and $y_m B x_1$, i.e., the path ϱ_0 is B -compatible with π_0 . As x_1By_m , by induction hypothesis, a path $\varrho_1 = (y'_j)_{j=m}^{m+k}$ from y_m for some $k \geq 0$ exists that is B -compatible with π_1 . Then the path $\varrho = (y_j)_{j=0}^{m+k}$ from y is B -compatible with $\pi = (x_i)_{i=0}^{\ell}$ as can be straightforwardly verified.

For the backward transfer condition (3), xBy and let $\pi = (x_i)_{i=0}^{\ell}$ be a path to x . We show by induction on ℓ that a B -compatible path ϱ to y exists. Basis, $\ell = 0$: The single point path $\varrho = (y)$ to y is B -compatible with π . Induction step, $\ell > 0$: Consider the path $\pi_0 = (x_{\ell-1}, x_{\ell})$ of length 1 to x and the path $\pi_1 = (x_i)_{i=0}^{\ell-1}$ of length $\ell - 1$ to $x_{\ell-1}$. Because by hypothesis $x_{\ell}By$ and $x_{\ell} \in \mathcal{C}(x_{\ell-1})$, since π is a path, we have, by property (3) of B , that a path $\varrho_0 = (y_j)_{j=0}^m$ to y exists for some $m \geq 0$ such that $y_0 B x_{\ell-1}$ and $y_j B x_{\ell}$ for all $j \in (0, m]$. Thus, path ϱ_0 is B -compatible with π_0 . As $x_{\ell-1}By_0$, by induction hypothesis, a path $\varrho_1 = (y'_j)_{j=0}^k$ to y_0 exists, for some $k \geq 0$, that is B -compatible with π_1 . Then, the path ϱ

$$\varrho(j) = \begin{cases} y'_j, & \text{if } j \in [0, k], \\ y_{j-k}, & \text{if } j \in (k, k+m]. \end{cases}$$

to y is B -compatible with π as can be straightforwardly verified. \square

The logic ICRL introduced in [CLMV22, CLMV25] provides a logical characterisation of CoPa-bisimilarity. Besides atomic propositions, negations, and conjunctions, the logic features two modalities, the forward modality $\vec{\zeta}$ and the backward modality $\bar{\zeta}$. Formulas Φ are given by

$$\Phi ::= p \mid \neg \Phi \mid \bigwedge_{i \in I} \Phi_i \mid \vec{\zeta} \Phi_1[\Phi_2] \mid \bar{\zeta} \Phi_1[\Phi_2]$$

Here, p ranges over \mathbf{AP} , and I ranges over a collection of finite and countably infinite index sets. The satisfaction relation of ICRL in a point x of a QdCM \mathcal{M} is

$$\begin{aligned}
 \mathcal{M}, x \models_{\text{ICRL}} p &\Leftrightarrow x \in \mathcal{V}(p) \\
 \mathcal{M}, x \models_{\text{ICRL}} \neg\Phi &\Leftrightarrow \mathcal{M}, x \not\models_{\text{ICRL}} \Phi \text{ does not hold} \\
 \mathcal{M}, x \models_{\text{ICRL}} \bigwedge_{i \in I} \Phi_i &\Leftrightarrow \mathcal{M}, x \models_{\text{ICRL}} \Phi_i \text{ for all } i \in I \\
 \mathcal{M}, x \models_{\text{ICRL}} \vec{\zeta}\Phi_1[\Phi_2] &\Leftrightarrow \text{a path } \pi \text{ and an index } \ell \text{ exist such that } \pi(0) = x, \\
 &\quad \mathcal{M}, \pi(\ell) \models_{\text{ICRL}} \Phi_1, \text{ and } \mathcal{M}, \pi(j) \models_{\text{ICRL}} \Phi_2 \text{ for } 0 \leq j < \ell \\
 \mathcal{M}, x \models_{\text{ICRL}} \overleftarrow{\zeta}\Phi_1[\Phi_2] &\Leftrightarrow \text{a path } \pi \text{ and an index } \ell \text{ exist such that } \pi(\ell) = x, \\
 &\quad \mathcal{M}, \pi(0) \models_{\text{ICRL}} \Phi_1, \text{ and } \mathcal{M}, \pi(j) \models_{\text{ICRL}} \Phi_2 \text{ for } 0 < j \leq \ell
 \end{aligned}$$

Logical equivalence \simeq_{ICRL} for ICRL is defined as expected: With respect to a QdCM \mathcal{M} , we have that points x and y are logically equivalent for ICRL, notation $x \simeq_{\text{ICRL}} y$, iff $\mathcal{M}, x \models_{\text{ICRL}} \Phi \Leftrightarrow \mathcal{M}, y \models_{\text{ICRL}} \Phi$. The following result, proven in [CLMV25], establishes the relationship between CoPa-bisimilarity and ICRL-equivalence.

Theorem 3.4. *For every QdCM \mathcal{M} it holds that ICRL-equivalence \simeq_{ICRL} coincides with CoPa-bisimilarity \equiv_{CoPa} . \square*

In the remainder of the paper, since we are concerned with finite models only, we confine to the finitary fragment of ICRL, i.e. the part where I is a finite index set.

In this work, given a QdCM $\mathcal{M} = (X, \mathcal{C}, \mathcal{V})$, we aim at running the spatial model checking algorithm of [CLLM16] on the quotient of \mathcal{M} with respect to \equiv_{CoPa} . The remainder of this paper is devoted to explain how to compute this quotient. It is a natural question at this point, whether the minimal model exists in the class of QdCMs. In other words, one needs to show that the set of equivalence classes of \equiv_{CoPa} can be endowed with a quasi-discrete closure operator, in such a way that logical truth is preserved and reflected. We do so in Theorem 3.5 below. With respect to \mathcal{M} , for a point $x \in X$, the notation $[x]$ is used to denote the equivalence class of x modulo \equiv_{CoPa} .

Theorem 3.5. *Given QdCS $\mathcal{M} = (X, \mathcal{C}, \mathcal{V})$, let $\tilde{\mathcal{M}} = (\tilde{X}, \tilde{\mathcal{C}}, \tilde{\mathcal{V}})$ where $\tilde{X} = X / \equiv_{\text{CoPa}}$, $\tilde{\mathcal{C}}([x]) = \{ [y'] \mid \exists y \in [x]: y' \in \mathcal{C}(y) \}$ for $x \in X$, and $\tilde{\mathcal{V}}(p) = \{ [x] \mid x \in \mathcal{V}(p) \}$ for $p \in \mathbf{AP}$. Then $\tilde{\mathcal{M}}$ is the smallest QdCS such that $\mathcal{M}, x \models \Phi \Leftrightarrow \tilde{\mathcal{M}}, [x] \models \Phi$ for $x \in X$, $\Phi \in \text{ICRL}$.*

Proof. Clearly, $\tilde{\mathcal{M}}$ is a QdCM. We verify by induction on the structure of a ICRL-formula Φ that $\mathcal{M}, x \models \Phi \Leftrightarrow \tilde{\mathcal{M}}, [x] \models \Phi$.

Case p : For $p \in \mathbf{AP}$, we have $\mathcal{M}, x \models p$ iff $x \in \mathcal{V}(p)$ iff $[x] \in \tilde{\mathcal{V}}(p)$ iff $\tilde{\mathcal{M}}, [x] \models p$.

Cases $\neg\Phi$ and $\Phi \wedge \Psi$: These cases follow directly from the induction hypothesis.

Case $\vec{\zeta}\Phi[\Psi]$: Suppose $\mathcal{M}, x \models \vec{\zeta}\Phi[\Psi]$. Let the path $\pi = (x_i)_{i=0}^\ell$ be such that $x_0 = x$, $\mathcal{M}, x_\ell \models \Phi$, and $\mathcal{M}, x_i \models \Psi$ for $0 \leq i < \ell$. Let $\tilde{\pi} = ([x_i])_{i=0}^\ell$. Then $[x_{i+1}] \in \tilde{\mathcal{C}}([x_i])$ since $x_{i+1} \in \mathcal{C}(x_i)$ for $0 \leq i < \ell$. So, $\tilde{\pi}$ is a path in \tilde{X} . Moreover, $[x_0] = [x]$, $\tilde{\mathcal{M}}, [x_\ell] \models \Phi$, and $\tilde{\mathcal{M}}, [x_i] \models \Psi$ for $0 \leq i < \ell$ by induction hypothesis for Φ and Ψ , respectively.

Reversely, suppose $\tilde{\mathcal{M}}, [x] \models \vec{\zeta}\Phi[\Psi]$. Let the path $\tilde{\pi} = ([\bar{x}_i])_{i=0}^\ell$, where $\bar{x}_i \in X$ for $0 \leq i \leq \ell$, be such that $[\bar{x}_0] = [x]$, $\tilde{\mathcal{M}}, [\bar{x}_\ell] \models \Phi$, and $\tilde{\mathcal{M}}, [\bar{x}_i] \models \Psi$ for $0 \leq i < \ell$. We proceed by induction on ℓ to show that, for some $m, k \geq 0$, a path $\pi = (y_j)_{j=0}^{m+k}$ exists with $y_0 = x$, $\mathcal{M}, y_{m+k} \models \Phi$, and $\mathcal{M}, y_j \models \Psi$ for $0 \leq j < m+k$. Basis, $\ell = 0$: Apparently,

$\tilde{\mathcal{M}}, [x] \models \Phi$. Hence, $\mathcal{M}, x \models \Phi$ by induction hypothesis for Φ . So, the single point path (x) fulfills the requirements.

Induction step, $\ell > 0$: We have $[\bar{x}_1] \in \tilde{\mathcal{C}}([\bar{x}_0])$. So, $\bar{x}'_0, \bar{x}'_1 \in X$ exist with $\bar{x}'_0 \rightleftharpoons_{\text{CoPa}} \bar{x}_0$, $\bar{x}'_1 \in \mathcal{C}(\bar{x}'_0)$, and $\bar{x}'_1 \rightleftharpoons_{\text{CoPa}} \bar{x}_1$. In view of the path (\bar{x}'_0, \bar{x}'_1) and $\bar{x}'_0 \rightleftharpoons_{\text{CoPa}} \bar{x}_0$, let the path $\pi_0 = (y_j)_{j=0}^m$ be such that $y_0 = x$, $y_j \rightleftharpoons_{\text{CoPa}} \bar{x}'_0$ for $0 \leq j < m$, and $y_m \rightleftharpoons_{\text{CoPa}} \bar{x}'_1$. Hence $y_j \rightleftharpoons_{\text{CoPa}} \bar{x}_0$ for $0 \leq j < m$. Because $\tilde{\mathcal{M}}, [\bar{x}_0] \models \Psi$, it follows that $\mathcal{M}, \bar{x}_0 \models \Psi$ by induction hypothesis for Ψ . So $\mathcal{M}, y_j \models \Psi$ for $0 \leq j < m$ by Theorem 3.4. Note, we have $\tilde{\mathcal{M}}, [\bar{x}_1] \models \zeta\tilde{\Phi}[\Psi]$ as witnessed by the path $([\bar{x}_i])_{i=1}^\ell$ of length $\ell-1$. So, $\mathcal{M}, \bar{x}_1 \models \zeta\tilde{\Phi}[\Psi]$ by induction hypothesis for ℓ . Therefore, $\mathcal{M}, y_m \models \zeta\tilde{\Phi}[\Psi]$ because $y_m \rightleftharpoons_{\text{CoPa}} \bar{x}'_1 \rightleftharpoons_{\text{CoPa}} \bar{x}_1$ and again Theorem 3.4. Let the path $\pi_1 = (y_j)_{j=m}^{m+k}$ from y_m be such that $\mathcal{M}, y_{m+k} \models \Phi$ and $\mathcal{M}, y_j \models \Psi$ for $m \leq j < m+k$. Then the combined path $\pi = (y_j)_{j=0}^{m+k}$ from x satisfies the required, and $\mathcal{M}, x \models \zeta\tilde{\Phi}[\Psi]$.

Case $\zeta\tilde{\Phi}[\Psi]$: Suppose $\mathcal{M}, x \models \zeta\tilde{\Phi}[\Psi]$. Let the path $\pi = (x_i)_{i=0}^\ell$ be such that $x_\ell = x$, $\mathcal{M}, x_0 \models \Phi$, and $\mathcal{M}, x_i \models \Psi$ for $0 < i \leq \ell$. Put $\tilde{\pi} = ([x_i])_{i=0}^\ell$. Then $[x_{i+1}] \in \tilde{\mathcal{C}}([x_i])$ since $x_{i+1} \in \mathcal{C}(x_i)$ for $0 \leq i < \ell$. Thus, $\tilde{\pi}$ is a path in \tilde{X} . Moreover, $[x_\ell] = [x]$, $\tilde{\mathcal{M}}, [x_0] \models \Phi$, and $\tilde{\mathcal{M}}, [x_i] \models \Psi$ for $0 < i \leq \ell$ by induction hypothesis for Φ and Ψ , respectively.

For the other direction, suppose $\tilde{\mathcal{M}}, [x] \models \zeta\tilde{\Phi}[\Psi]$. Let the path $\tilde{\pi} = ([\bar{x}_i])_{i=0}^\ell$, where $\bar{x}_i \in X$ for $0 \leq i \leq \ell$, be such that $[\bar{x}_\ell] = [x]$, $\tilde{\mathcal{M}}, [\bar{x}_0] \models \Phi$, and $\tilde{\mathcal{M}}, [\bar{x}_i] \models \Psi$ for $0 < i \leq \ell$.

We proceed by induction on ℓ to verify that, for some $k, m \geq 0$, a path $\pi = (y_j)_{j=0}^{k+m}$ to x exists with $\mathcal{M}, y_0 \models \Phi$ and $\mathcal{M}, y_j \models \Psi$ for $0 < j \leq k+m$. Basis, $\ell = 0$: The single point path (x) fulfills the requirements, as apparently, $\tilde{\mathcal{M}}, [x] \models \Phi$ and therefore $\mathcal{M}, x \models \Phi$ by induction hypothesis for Φ .

Induction step, $\ell > 0$: We have $[\bar{x}_\ell] \in \tilde{\mathcal{C}}([\bar{x}_{\ell-1}])$. Therefore, we can find $\bar{x}'_{\ell-1}, \bar{x}'_\ell \in X$ with $\bar{x}'_{\ell-1} \rightleftharpoons_{\text{CoPa}} \bar{x}_{\ell-1}$, $\bar{x}'_\ell \in \mathcal{C}(\bar{x}'_{\ell-1})$, and $\bar{x}'_\ell \rightleftharpoons_{\text{CoPa}} \bar{x}_\ell$. In view of the path $(\bar{x}'_{\ell-1}, \bar{x}'_\ell)$ and $\bar{x}'_{\ell-1} \rightleftharpoons_{\text{CoPa}} \bar{x}_{\ell-1}$, let the path $\pi'' = (y''_j)_{j=0}^m$ to \bar{x}_ℓ be such that $y''_0 \rightleftharpoons_{\text{CoPa}} \bar{x}'_{\ell-1}$, $y''_j \rightleftharpoons_{\text{CoPa}} \bar{x}'_\ell$ for $0 < j \leq m$. Hence $y''_j \rightleftharpoons_{\text{CoPa}} \bar{x}_\ell$ for $0 < j \leq m$. Because $\tilde{\mathcal{M}}, [\bar{x}_\ell] \models \Psi$, we have $\mathcal{M}, \bar{x}_\ell \models \Psi$ by induction hypothesis for Ψ and $\mathcal{M}, y''_j \models \Psi$ for $0 < j \leq m$ by Theorem 3.4. Note, we have $\tilde{\mathcal{M}}, [\bar{x}_{\ell-1}] \models \zeta\tilde{\Phi}[\Psi]$ as witnessed by the path $([\bar{x}_i])_{i=0}^{\ell-1}$ of length $\ell-1$. So, $\mathcal{M}, \bar{x}_{\ell-1} \models \zeta\tilde{\Phi}[\Psi]$ by induction hypothesis for ℓ . Therefore, $\mathcal{M}, y''_0 \models \zeta\tilde{\Phi}[\Psi]$ because $y''_0 \rightleftharpoons_{\text{CoPa}} \bar{x}'_{\ell-1} \rightleftharpoons_{\text{CoPa}} \bar{x}_{\ell-1}$ and another application of Theorem 3.4. Let the path $\pi' = (y'_j)_{j=0}^k$ to y''_0 be such that $\mathcal{M}, y'_0 \models \Phi$ and $\mathcal{M}, y'_j \models \Psi$ for $0 < j \leq k$. Let the combined path $\pi = (y_j)_{j=0}^{k+m}$ be given by $y_j = y'_j$ for $0 \leq j \leq k$ and $y_j = y''_{j-k}$ for $0 \leq j \leq m$. Note, $y'_k = y''_0$. Then the path π is as required: It holds that $\mathcal{M}, y_0 \models \Phi$ as $y_0 = y'_0$. Moreover, $\mathcal{M}, y_j \models \Psi$ for $0 < j \leq k$ and $k < j \leq k+m$ as $\mathcal{M}, y'_j \models \Psi$ for $0 < j \leq k$ and $\mathcal{M}, y''_{j-k} \models \Psi$ for $k < j \leq k+m$, respectively. Finally, $y_{k+m} = y''_m = \bar{x}_\ell = x$. Thus, path π is a path to x that witnesses $\mathcal{M}, x \models \zeta\tilde{\Phi}[\Psi]$, as was to be shown.

As to $\tilde{\mathcal{M}}$ being the QdCM with the smallest number of elements, suppose $\mathcal{N} = (Y, \mathcal{D}, \mathcal{W})$ is a QdCM and $f : X \rightarrow Y$ is a surjection such that $\mathcal{M}, x \models \Phi \Leftrightarrow \mathcal{N}, f(x) \models \Phi$ for $x \in X$, $\Phi \in \text{ICRL}$. Define the mapping $g : Y \rightarrow \tilde{X}$ by $g(y) = [x]$ if $f(x) = y$. This is well-defined: If $f(x) = f(x')$, then $x \simeq_{\text{ICRL}} x'$ by the assumed property of \mathcal{N} . Thus, $x \rightleftharpoons_{\text{CoPa}} x'$ by Theorem 3.4 and $[x] = [x']$. By surjectivity of f , also g is surjective. Therefore, $|Y| \geq |\tilde{X}|$. \square

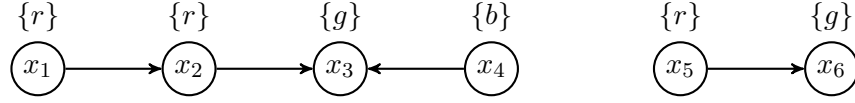


FIGURE 5. A finite QdCM

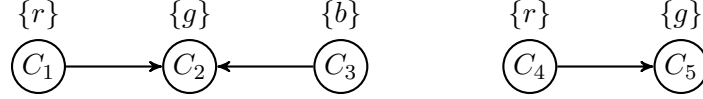


FIGURE 6. Minimal QdCM of the QdCM of Figure 5.

Example 3.6. Consider the simple QdCM in Figure 5. It has five equivalence classes, namely $C_1 = \{x_1, x_2\}$, $C_2 = \{x_3\}$, $C_3 = \{x_4\}$, $C_4 = \{x_5\}$, and $C_5 = \{x_6\}$. To verify this, it is in view of Theorem 3.4 convenient to use logical equivalence rather than CoPa-bisimilarity. The points x_1 and x_2 are in the same class, but x_5 is not in that class. This is so because from x_1 and x_2 , that satisfy the same atomic proposition r , one can reach point x_3 , labelled by g that, in turn, can be *reached from* x_4 which is labelled by b . This does not hold for x_5 . The formula that distinguishes x_1 (and x_2) from x_5 is $\vec{\zeta}(\vec{\zeta}b[g])[r]$. In fact, from x_4 there is a path π , with $\pi(0) = x_4$, labelled by b , and with $\pi(1) = x_3$, labelled by g , so x_3 satisfies $\vec{\zeta}b[g]$. This formula is not satisfied by x_6 since there is no path, starting in a point with label b and then going to x_6 . Furthermore, there is a path π' , with $\pi'(0) = x_1$, $\pi'(1) = x_2$ and $\pi'(2) = x_3$, so x_1 (and x_2) satisfy $\vec{\zeta}(\vec{\zeta}b[g])[r]$. Also x_3 and x_6 , both labelled by g are not in the same class because, as we have seen, x_3 can be reached from a point satisfying b , but x_6 cannot. The minimal model, applying Theorem 3.5, is shown in Figure 6.

We close this section remarking that if a QdCM \mathcal{M} is symmetric, i.e., the relation R underlying the closure operator of \mathcal{M} is a symmetric relation, then $\mathcal{M}, x \models_{\text{ICRL}} \vec{\zeta}\Phi_1[\Phi_2]$ if and only if $\mathcal{M}, x \models_{\text{ICRL}} \vec{\zeta}\Phi_1[\Phi_2]$, for all $x \in \mathcal{M}$ and ICRL formulas Φ_1 and Φ_2 .

4. FROM QDCMS TO LABELLED TRANSITION SYSTEMS

In this section we show how a finite QdCM can be encoded as an LTS in such a way that CoPa-bisimilarity in the QdCM is preserved and reflected by branching bisimilarity in the LTS: two points in the QdCM are mapped to branching bisimilar states in the LTS precisely when the two points are CoPa-bisimilar in the first place. We first present the encoding for general QdCSs, i.e., QdCSs that may or may not be symmetric. Next, the encoding for symmetric QdCSs is given. Because of the symmetry in these models, a more compact encoding is possible.

4.1. LTS encoding of general QdCSs.

The idea of the encoding of a QdCM $\mathcal{M} = (X, \mathcal{C}, \mathcal{V})$ that is not necessarily symmetric is as follows: (i) each element $x \in X$ corresponds to exactly two states in the LTS, a forward

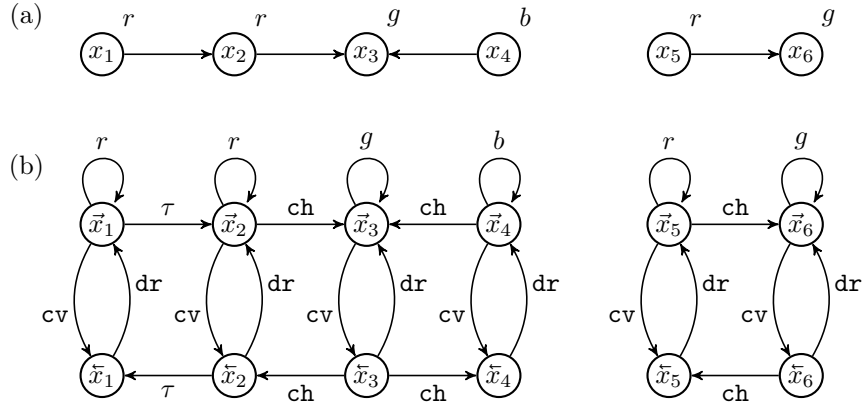


FIGURE 7. (a) QdCM of Figure 5 repeated; (b) its encoding as LTS, where τ -selfloops are omitted for readability reasons.

state \vec{x} and a backward state \tilde{x} that have transitions back and forth between them labelled cv and dr , standing for “converse” and “direct”, (ii) for each proposition letter p that is satisfied in the QdCM by x there is a selfloop in the forward state \vec{x} labelled by p , (iii) there are τ -transitions between two forward states \vec{x} and \vec{x}' and between two backward states \tilde{x} and \tilde{x}' if x and x' satisfy the same proposition letters, and (iv) between two forward states \vec{x} and \vec{x}' — respectively, two backward states \tilde{x} and \tilde{x}' — there are transitions with a special label ch , indicating change, if x and x' do not satisfy the same proposition letters.

Definition 4.1 (Encoding, general case). Let $\mathcal{M} = (X, \mathcal{C}, \mathcal{V})$ be a finite CM. Define labelled transition system $LTS_{gen}(\mathcal{M}) = (S, \mathcal{A}, \rightarrow)$ by

- (i) $S = \{ \vec{x}, \tilde{x} \mid x \in X \}$;
- (ii) $\mathcal{A} = AP \cup \{cv, dr, ch, \tau\}$ with cv, dr, ch, τ fresh labels;
- (iii) $\rightarrow \subseteq S \times \mathcal{A} \times S$ such that

$$\begin{aligned}
 & \vec{x} \xrightarrow{p} \vec{x} && \text{for } x \in X, p \in AP \text{ such that } x \in \mathcal{V}(p) \\
 & \vec{x} \xrightarrow{cv} \tilde{x}, \tilde{x} \xrightarrow{dr} \vec{x} && \text{for } x \in X \\
 & \vec{x} \xrightarrow{\tau} \vec{x}', \tilde{x}' \xrightarrow{\tau} \tilde{x} && \text{for } x, x' \in X \text{ such that } x' \in \mathcal{C}(x) \text{ and } x =_{\mathcal{V}} x' \\
 & \vec{x} \xrightarrow{ch} \vec{x}', \tilde{x}' \xrightarrow{ch} \tilde{x} && \text{for } x, x' \in X \text{ such that } x' \in \mathcal{C}(x) \text{ and } x \neq_{\mathcal{V}} x'
 \end{aligned}$$

Example 4.2. Figure 7 depicts at the top the QdCM of Figure 5 and at the bottom its encoding as LTS. Its six elements x_1, \dots, x_6 give rise to the states $\vec{x}_1, \dots, \vec{x}_6$ and $\tilde{x}_1, \dots, \tilde{x}_6$ with transitions with label cv and dr between them. Since the elements x_1, x_2 , and x_5 satisfy proposition letter r , the states \vec{x}_1, \vec{x}_2 , and \vec{x}_5 have a selfloop with label r . Similarly, the elements x_3 and x_6 with proposition letter g yield the selfloops with label g for \vec{x}_3 and \vec{x}_6 , the element x_4 with proposition letter b yields the selfloop with label b . As indicated by the arrow, we have that $x_1 \in \mathcal{C}(x_2)$. Moreover, both x_1 and x_2 satisfy proposition letter r only. So, in the LTS we have the transitions $\vec{x}_1 \xrightarrow{\tau} \vec{x}_2$ and $\tilde{x}_2 \xrightarrow{\tau} \tilde{x}_1$. Since $x_2, x_4 \in \mathcal{C}(x_3)$ and $x_5 \in \mathcal{C}(x_6)$ and different proposition letters are satisfied by the pairs of elements, we

have **ch**-transitions $\vec{x}_2 \xrightarrow{\text{ch}} \vec{x}_3$, $\vec{x}_4 \xrightarrow{\text{ch}} \vec{x}_3$, and $\vec{x}_5 \xrightarrow{\text{ch}} \vec{x}_6$ and their counterparts $\vec{x}_3 \xrightarrow{\text{ch}} \vec{x}_2$, $\vec{x}_3 \xrightarrow{\text{ch}} \vec{x}_4$, and $\vec{x}_6 \xrightarrow{\text{ch}} \vec{x}_5$.

Below, Theorem 4.5 states that CoPa-bisimilarity of two elements of a closure model \mathcal{M} coincides with branching bisimilarity of their corresponding states in $\text{LTS}_{\text{gen}}(\mathcal{M})$. In preparation of the proof the theorem we first establish two lemmas regarding the structure of $\text{LTS}_{\text{gen}}(\mathcal{M})$. In turn, in aid of proving the first lemma, we introduce the notion of the depth of a state in an LTS and note a number of properties of it.

Let a finite LTS $\mathcal{S} = (S, \mathcal{A}, \rightarrow)$ and an action $\tau \in \mathcal{A}$ be given. For $s \in S$, we define the depth $|s|$ of s in \mathcal{S} by

$$|s| = \max\{n \in \mathbb{N} \mid \exists s_0, \dots, s_n \in S : \forall i, 0 \leq i < n : (s_i \xrightarrow{\tau} s_{i+1}) \wedge \neg(s_{i+1} \xrightarrow{\tau} s_i)\}$$

By finiteness of S , the above is well-defined; in the sequence s_0, \dots, s_n each state s_i can only occur once.

For $s, t \in S$ we define $s \equiv_{\tau} t$ iff $(s \xrightarrow{\tau} t) \wedge (t \xrightarrow{\tau} s)$. A straightforward verification shows that the relation $\equiv_{\tau} \subseteq S \times S$ is a branching bisimulation relation on \mathcal{S} . Therefore, (i) $s \equiv_{\tau} t$ implies $s \leftrightarrow_b t$. Also, (ii) if $|s| = |t|$ and $s \xrightarrow{\tau} t$ then we have $s \equiv_{\tau} t$. For, if $s \not\equiv_{\tau} t$, we have $\neg(t \xrightarrow{\tau} s)$ and $|s| > |t|$ would follow. Thus, (iii) if $|s| = 0$ and $s \xrightarrow{\tau} t$ it follows that $s \equiv_{\tau} t$. Finally, from the definition of depth one directly obtains that (iv) $s \xrightarrow{\tau} t$ implies $|s| \geq |t|$.

Lemma 4.3. *Let $\mathcal{M} = (X, \mathcal{C}, \mathcal{V})$ be a finite CM. For $x \in X$, it holds in $\text{LTS}_{\text{gen}}(\mathcal{M})$ that*

$$\text{if } \vec{x} \xrightarrow{\tau} \vec{x}' \text{ and } \vec{x} \leftrightarrow_b \vec{x}' \text{ then } \vec{x}' \xrightarrow{\tau} \vec{x} \text{ and } \vec{x} \leftrightarrow_b \vec{x}'$$

Proof. For $x, x' \in X$, if $\vec{x} \xrightarrow{\tau} \vec{x}'$ then $\vec{x}' \xrightarrow{\tau} \vec{x}$ by construction of $\text{LTS}_{\text{gen}}(\mathcal{M})$. We verify the conclusion $\vec{x} \leftrightarrow_b \vec{x}'$ of the lemma by induction on the depth $|\vec{x}|$.

Basis, $|\vec{x}| = 0$: Because $|\vec{x}| = 0$ and $\vec{x} \xrightarrow{\tau} \vec{x}'$, we have by (iii) that $\vec{x} \equiv_{\tau} \vec{x}'$. By construction of $\text{LTS}_{\text{gen}}(\mathcal{M})$, $\vec{x}' \equiv_{\tau} \vec{x}$, and therefore $\vec{x}' \leftrightarrow_b \vec{x}$ by (i).

Induction step, $|\vec{x}| > 0$: Assume $\vec{x} \xrightarrow{\tau} \vec{x}'$ and $\vec{x} \leftrightarrow_b \vec{x}'$. We have $\vec{x} \xrightarrow{\text{cv}} \vec{x}$ by construction of $\text{LTS}_{\text{gen}}(\mathcal{M})$. Because $\vec{x} \leftrightarrow_b \vec{x}'$, a matching computation for \vec{x}' exists, $\vec{x}' = \vec{u}_0 \xrightarrow{\tau} \dots \xrightarrow{\tau} \vec{u}_n \xrightarrow{\text{cv}} \vec{u}_n$ say, where $n \geq 0$ and $u_0, \dots, u_n \in X$ are such that $\vec{u}_i \leftrightarrow_b \vec{x}$ for $0 \leq i \leq n$ and $\vec{u}_n \leftrightarrow_b \vec{x}$. (Note that $\vec{u}_0, \dots, \vec{u}_n$ rather than $\tilde{u}_0, \dots, \tilde{u}_n$ are involved, since τ -transitions preserve direction, *i.e.*, if $s \xrightarrow{\tau} t$ in $\text{LTS}_{\text{gen}}(\mathcal{M})$ then either $s = \vec{x}, t = \vec{y}$ or $s = \vec{x}, t = \vec{y}$, for suitable $x, y \in X$.) Since $\vec{u}_0 \xrightarrow{\tau} \dots \xrightarrow{\tau} \vec{u}_n$, it holds by (iv) that $|\vec{u}_0| \geq \dots \geq |\vec{u}_n|$. We distinguish two cases.

Case I, $|\vec{u}_0| = |\vec{u}_n|$: We have $\vec{u}_0 \equiv_{\tau} \vec{u}_n$ by (ii). So, $\vec{u}_0 \leftrightarrow_b \vec{u}_n$ by (i) and hence $\vec{u}_0 \leftrightarrow_b \vec{u}_n$ by construction of $\text{LTS}_{\text{gen}}(\mathcal{M})$. Using $\vec{x}' = \vec{u}_0$ and $\vec{u}_n \leftrightarrow_b \vec{x}$ it follows that $\vec{x}' \leftrightarrow_b \vec{u}_0 \leftrightarrow_b \vec{u}_n \leftrightarrow_b \vec{x}$.

Case II, $|\vec{u}_0| \neq |\vec{u}_n|$: We have $|\vec{u}_0| > |\vec{u}_n|$ by (iv). Let $k, 0 \leq k < n$, be the minimal index such that $|\vec{u}_k| > |\vec{u}_{k+1}|$. By hypothesis $\vec{x} \xrightarrow{\tau} \vec{x}'$. So, $|\vec{x}| \geq |\vec{x}'| = |\vec{u}_0| = |\vec{u}_k| > |\vec{u}_\ell|$ for $k+1 \leq \ell \leq n$. By choice of u_n we have

$$\vec{x} \leftrightarrow_b \vec{u}_n \tag{4.1}$$

Because $\vec{u}_{k+1} \xrightarrow{\tau} \dots \xrightarrow{\tau} \vec{u}_n$ and $\vec{u}_{k+1} \leftrightarrow_b \dots \leftrightarrow_b \vec{u}_n$, it follows by induction hypothesis that $\vec{u}_{k+1} \leftrightarrow_b \dots \leftrightarrow_b \vec{u}_n$. Hence,

$$\vec{u}_n \leftrightarrow_b \vec{u}_{k+1} \tag{4.2}$$

Since $\vec{u}_k \leftrightarrow_b \vec{u}_{k+1}$ and $\vec{u}_k \xrightarrow{\text{dr}} \vec{u}_k$, a matching sequence for \vec{u}_{k+1} exists, which is, by definition of $\text{LTS}_{\text{gen}}(\mathcal{M})$, of the form $\vec{u}_{k+1} = \vec{v}_0 \xrightarrow{\tau} \dots \xrightarrow{\tau} \vec{v}_m \xrightarrow{\text{dr}} \vec{v}_m$ for suitable $m \geq 0$ and

$v_0, \dots, v_m \in X$ such that $\vec{v}_0, \dots, \vec{v}_m \leftrightarrow_b \vec{u}_k$ and $\vec{v}_m \leftrightarrow_b \vec{u}_k$. From $\vec{u}_{k+1} \xrightarrow{\tau^*} \vec{v}_j$ we get, by (iv) that $|\vec{u}_{k+1}| \geq |\vec{v}_j|$ for $0 \leq j \leq m$. Moreover, we know that $|\vec{x}| \geq |\vec{u}_0| = |\vec{u}_k| > |\vec{u}_{k+1}|$. Thus, we get that $|\vec{x}| \geq |\vec{u}_0| = |\vec{u}_k| > |\vec{u}_{k+1}| \geq |\vec{v}_j|$ for $0 \leq j \leq m$. By induction hypothesis we obtain $\vec{u}_{k+1} \leftrightarrow_b \vec{v}_0, \dots, \vec{v}_m$. In particular,

$$\vec{u}_{k+1} \leftrightarrow_b \vec{v}_m \quad (4.3)$$

By choice of v_m we have

$$\vec{v}_m \leftrightarrow_b \vec{u}_k \quad (4.4)$$

Finally, from $|\vec{x}'| = |\vec{u}_0| = |\vec{u}_k|$ and $\vec{x}' = \vec{u}_0 \xrightarrow{\tau^*} \vec{u}_k$ one derives $\vec{x}' \equiv_{\tau} \vec{u}_k$ using (ii). Therefore, $\vec{x}' \equiv_{\tau} \vec{u}_k$, which implies

$$\vec{x}' \leftrightarrow_b \vec{u}_k \quad (4.5)$$

by (i). Combining equations (4.1) to (4.5) gives $\vec{x} \leftrightarrow_b \vec{u}_n \leftrightarrow_b \vec{u}_{k+1} \leftrightarrow_b \vec{v}_m \leftrightarrow_b \vec{u}_k \leftrightarrow_b \vec{x}'$. So $\vec{x} \leftrightarrow_b \vec{x}'$, as was to be shown. \square

The next lemma states branching bisimilarity of pairs of forward states and of backward states in an encoding LTS are related.

Lemma 4.4. *Let $\mathcal{M} = (X, \mathcal{C}, \mathcal{V})$ be a finite CM. Then $\vec{x} \leftrightarrow_b \vec{y} \Leftrightarrow \vec{x} \leftrightarrow_b \vec{y}$ in $\text{LTS}_{\text{gen}}(\mathcal{M})$ for $x, y \in X$.*

Proof. (\Rightarrow) Let $x, y \in X$ such that $\vec{x} \leftrightarrow_b \vec{y}$. For the transition $\vec{x} \xrightarrow{\text{cv}} \vec{x}$ of \vec{x} , a matching computation of \vec{y} exists, which is of the form $\vec{y} = \vec{u}_0 \xrightarrow{\tau} \vec{u}_1 \xrightarrow{\tau} \dots \xrightarrow{\tau} \vec{u}_n \xrightarrow{\text{cv}} \vec{u}_n$ by definition of $\text{LTS}_{\text{gen}}(\mathcal{M})$ and satisfies $\vec{u}_0, \dots, \vec{u}_n \leftrightarrow_b \vec{x}$ and $\vec{u}_n \leftrightarrow_b \vec{x}$. Repeated application of Lemma 4.3 yields $\vec{u}_n \xrightarrow{\tau} \dots \xrightarrow{\tau} \vec{u}_0 = \vec{y}$ and $\vec{u}_n \leftrightarrow_b \vec{y}$. Thus $\vec{x} \leftrightarrow_b \vec{u}_n \leftrightarrow_b \vec{y}$, as was to be shown. (\Leftarrow) Similar to the above. \square

The encoding of Definition 4.1 preserves CoPa-bisimilarity of a QdCM \mathcal{M} and reflects branching bisimilarity of the LTS $\text{LTS}_{\text{gen}}(\mathcal{M})$.

Theorem 4.5. *Let $\mathcal{M} = (X, \mathcal{C}, \mathcal{V})$ be a finite CM. For $x, y \in X$, it holds that*

$$x \rightleftharpoons_{\text{CoPa}} y \text{ in } \mathcal{M} \text{ iff } \vec{x} \leftrightarrow_b \vec{y} \text{ in } \text{LTS}_{\text{gen}}(\mathcal{M})$$

Proof. (\Leftarrow) Define the relation $B \subseteq X \times X$ by xBy if $\vec{x} \leftrightarrow_b \vec{y}$ for $x, y \in X$. We verify that the relation B is a CoPa-bisimulation using Lemma 3.3. Suppose $x, y \in X$ satisfy xBy . Thus $\vec{x} \leftrightarrow_b \vec{y}$.

(i) Let $p \in \text{AP}$. If $x \in \mathcal{V}(p)$, then $\vec{x} \xrightarrow{p} \vec{x}$ in $\text{LTS}_{\text{gen}}(\mathcal{M})$. Since $\vec{x} \leftrightarrow_b \vec{y}$ in $\text{LTS}_{\text{gen}}(\mathcal{M})$, exist $s, t \in S$ such that $\vec{y} \xrightarrow{\tau^*} s \xrightarrow{p} t$ with $s, t \leftrightarrow_b \vec{x}$. By definition of $\text{LTS}_{\text{gen}}(\mathcal{M})$, it must be that $s, t = \vec{y}'$ for some $y' \in \mathcal{V}(p)$. Moreover, $\vec{y} \xrightarrow{\tau^*} \vec{y}'$ implies, again by definition of $\text{LTS}_{\text{gen}}(\mathcal{M})$, that $y =_{\mathcal{V}} y'$. Hence $y \in \mathcal{V}(p)$. Symmetrically, $y \in \mathcal{V}(p)$ implies $x \in \mathcal{V}(p)$. So, we conclude $x =_{\mathcal{V}} y$.

(ii) Suppose $x' \in \mathcal{C}(x)$ for some $x' \in X$. It suffices to show that a path $(y_i)_{i=0}^n$ from y exists such that xBy_i for $0 \leq i < n$ and $x'B y_n$. The assumption $x' \in \mathcal{C}(x)$ implies that $\text{LTS}_{\text{gen}}(\mathcal{M})$ has either the transition $\vec{x} \xrightarrow{\tau} \vec{x}'$ or the transition $\vec{x} \xrightarrow{\text{ch}} \vec{x}'$. In the case of a τ -transition, by branching bisimilarity of \vec{x} and \vec{y} , a computation $\vec{y}_0 \xrightarrow{\tau} \dots \xrightarrow{\tau} \vec{y}_n$ from \vec{y} with $n \geq 0$ exists such that $\vec{x} \leftrightarrow_b \vec{y}_0, \dots, \vec{y}_{n-1}$ and $\vec{x}' \leftrightarrow_b \vec{y}_n$. If $n > 0$, by definition of $\text{LTS}_{\text{gen}}(\mathcal{M})$, it holds that $y_{i+1} \in \mathcal{C}(y_i)$ for $0 \leq i < n$. So, $(y_i)_{i=0}^n$ is a path from y in X as required. If $n = 0$, we have both xBy and $x'B y$, and then the two elements path (y, y) is a path from y in X as required. In the case of a ch -transition, by branching bisimilarity

of \vec{x} and \vec{y} , a computation $y_0 \xrightarrow{\tau} \cdots \xrightarrow{\tau} y_{n-1} \xrightarrow{\text{ch}} y_n$ from \vec{y} with $n \geq 1$ exists such that $\vec{x} \xleftrightarrow{b} y_0, \dots, y_{n-1}$ and $\vec{x}' \xleftrightarrow{b} y_n$. Also here by definition of $\text{LTS}_{\text{gen}}(\mathcal{M})$, $(y_i)_{i=0}^n$ is a path from y in X as required.

(iii) Now suppose $x \in \mathcal{C}(x')$ for some $x' \in X$. We have to show that a path $(y_i)_{i=0}^n$ to y exists such that $x'By_0$ and xBy_i for $0 < i \leq n$. We will use that $\vec{x} \xleftrightarrow{b} \vec{y}$, which follows from $\vec{x} \xleftrightarrow{b} \vec{y}$ by Lemma 4.4. It holds that in $\text{LTS}_{\text{gen}}(\mathcal{M})$ either the transition $\vec{x} \xrightarrow{\tau} \vec{x}'$ or the transition $\vec{x} \xrightarrow{\text{ch}} \vec{x}'$ exists. In the case of a τ -transition, by branching bisimilarity of \vec{x} and \vec{y} , $\text{LTS}_{\text{gen}}(\mathcal{M})$ has a computation $\vec{y}_0 \xrightarrow{\tau} \cdots \xrightarrow{\tau} \vec{y}_n$ from \vec{y} with $n \geq 0$ such that $\vec{x} \xleftrightarrow{b} \vec{y}_0, \dots, \vec{y}_{n-1}$ and $\vec{x}' \xleftrightarrow{b} \vec{y}_n$. Lemma 4.4 yields $\vec{x} \xleftrightarrow{b} \vec{y}_0, \dots, \vec{y}_{n-1}$ and $\vec{x}' \xleftrightarrow{b} \vec{y}_n$, thus xBy_i for $0 \leq i < n$ and $x'By_n$. Note, by definition of $\text{LTS}_{\text{gen}}(\mathcal{M})$, $y_i \in \mathcal{C}(y_{i+1})$ for $0 \leq i < n$. Therefore, if $n > 0$ then, in reverse order, $(y_{n-i})_{i=0}^n$ is a path to y in X as required. If $n = 0$, we have both $x'By$ and xBy . Consequently, the path (y, y) is a path to y in X satisfying what is required. In the case of a ch -transition, by branching bisimilarity of \vec{x} and \vec{y} , a computation $\vec{y}_0 \xrightarrow{\tau} \cdots \xrightarrow{\tau} \vec{y}_{n-1} \xrightarrow{\text{ch}} \vec{y}_n$ from \vec{y} with $n \geq 1$ exists such that $\vec{x} \xleftrightarrow{b} \vec{y}_0, \dots, \vec{y}_{n-1}$ and $\vec{x}' \xleftrightarrow{b} \vec{y}_n$. Again we obtain $\vec{x} \xleftrightarrow{b} \vec{y}_0, \dots, \vec{y}_{n-1}$ and $\vec{x}' \xleftrightarrow{b} \vec{y}_n$, thus xBy_i for $0 \leq i < n$ and $x'By_n$ by application of Lemma 4.4. Moreover, $y_i \in \mathcal{C}(y_{i+1})$ for $0 \leq i < n$ by definition of $\text{LTS}_{\text{gen}}(\mathcal{M})$. Thus, we have that, again in reversed order, $(y_{n-i})_{i=0}^n$ is a path to y in X as required.

(\Leftarrow) We verify that the relation $B \subseteq S \times S$ given by $B = \{ (\vec{x}, \vec{y}), (\vec{x}, \vec{y}) \mid x \rightleftharpoons_{\text{CoPa}} y \}$ is a branching bisimulation relation on $\text{LTS}_{\text{gen}}(\mathcal{M})$. Suppose $x, y \in X$ satisfy $x \rightleftharpoons_{\text{CoPa}} y$.

We check that each transition of \vec{x} can be matched by \vec{y} . (i) If $\vec{x} \xrightarrow{p} \vec{x}$ for some proposition $p \in \text{AP}$, then $x \in \mathcal{V}(p)$. Hence, by CoPa-bisimilarity, $y \in \mathcal{V}(p)$. So, $\vec{y} \xrightarrow{p} \vec{y}$, and the single-step computation $\vec{y} \xrightarrow{p} \vec{y}$ in $\text{LTS}_{\text{gen}}(\mathcal{M})$ matches the transition $\vec{x} \xrightarrow{p} \vec{x}$. (ii) The transition $\vec{x} \xrightarrow{\text{cv}} \vec{x}$ is matched by the single-step computation $\vec{y} \xrightarrow{\text{cv}} \vec{y}$, by construction of $\text{LTS}_{\text{gen}}(\mathcal{M})$. (iii) If $\vec{x} \xrightarrow{\tau} \vec{x}'$ for some $x' \in X$, then $x' \in \mathcal{C}(x)$ and $x =_{\mathcal{V}} x'$. Thus, (x, x') is a path from x in X . By CoPa-bisimilarity of x and y , it follows that in X a path $(y_i)_{i=0}^n$ from y exists such that $x \rightleftharpoons_{\text{CoPa}} y_0, \dots, y_{n-1}$ and $x' \rightleftharpoons_{\text{CoPa}} y_n$. Then we have $x =_{\mathcal{V}} y_0, \dots, y_{n-1}$ and also $x =_{\mathcal{V}} x' =_{\mathcal{V}} y_n$. Thus, both $y_{i+1} \in \mathcal{C}(y_i)$ and $y_i =_{\mathcal{V}} y_{i+1}$ for $0 \leq i < n$. Hence, in $\text{LTS}_{\text{gen}}(\mathcal{M})$ we have a computation $\vec{y}_0 \xrightarrow{\tau} \cdots \xrightarrow{\tau} \vec{y}_n$ such that $\vec{x}B\vec{y}_i$ for $0 \leq i < n$ and $\vec{x}'B\vec{y}_n$. Therefore, \vec{y} matches with this computation the τ -transition of \vec{x} . (iv) Similarly, if $\vec{x} \xrightarrow{\text{ch}} \vec{x}'$ for some $x' \in X$, then we find in $\text{LTS}_{\text{gen}}(\mathcal{M})$ a computation $\vec{y}_0 \xrightarrow{\tau} \cdots \xrightarrow{\tau} \vec{y}_{n-1} \xrightarrow{\text{ch}} \vec{y}_n$ from \vec{y} which matches the ch -transition of \vec{x} .

Next we check that each transition of \vec{x} can be matched by a computation of \vec{y} . (i) The transition $\vec{x} \xrightarrow{\text{dr}} \vec{x}$ is matched by the single-step computation $\vec{y} \xrightarrow{\text{dr}} \vec{y}$. (ii) If $\vec{x} \xrightarrow{\tau} \vec{x}'$ for some $x' \in X$, a reasoning similar to the corresponding case for \vec{x} applies. By definition of $\text{LTS}_{\text{gen}}(\mathcal{M})$, it holds that $x \in \mathcal{C}(x')$ and $x =_{\mathcal{V}} x'$. Thus, (x', x) is a path to x in X . By CoPa-bisimilarity of x and y , it follows that in X a path $(y_i)_{i=0}^n$ to y exists that satisfies $x' \rightleftharpoons_{\text{CoPa}} y_0$ and $x \rightleftharpoons_{\text{CoPa}} y_1, \dots, y_n$. Then we have $x =_{\mathcal{V}} x' =_{\mathcal{V}} y_0$ and also $x =_{\mathcal{V}} y_i$ for $0 < i \leq n$. Thus, both $y_{i+1} \in \mathcal{C}(y_i)$ and $y_i =_{\mathcal{V}} y_{i+1}$ for $0 \leq i < n$. Hence, by definition of $\text{LTS}_{\text{gen}}(\mathcal{M})$, a computation $\vec{y}_n \xrightarrow{\tau} \cdots \xrightarrow{\tau} \vec{y}_0$ of \vec{y} exists which satisfies $\vec{x}B\vec{y}_i$ for $n \geq i > 0$ and $\vec{x}'B\vec{y}_0$. Therefore, this computation of \vec{y} matches the τ -transition of \vec{x} . (iii) Finally, a transition $\vec{x} \xrightarrow{\text{ch}} \vec{x}'$ for some $x' \in X$ is matched by \vec{y} . In fact, if $\vec{x} \xrightarrow{\text{ch}} \vec{x}'$ for some $x' \in X$, then it holds that $x \in \mathcal{C}(x')$ and $x \neq_{\mathcal{V}} x'$. Thus (x', x) is a path to x in \mathcal{M} . Let by CoPa-bisimilarity of x and y , the path $(y_i)_{i=0}^n$ be a matching path to y . Note $n \geq 1$ as

$x \not\equiv_{\text{CoPa}} x'$. We have $x' \equiv_{\text{CoPa}} y_0$ and $x \equiv_{\text{CoPa}} y_1, \dots, y_n$. Thus, $y_0 =_{\mathcal{V}} x' \neq_{\mathcal{V}} x =_{\mathcal{V}} y_1$ and $y_1 =_{\mathcal{V}} \dots =_{\mathcal{V}} y_n$. So, in $\text{LTS}_{\text{gen}}(\mathcal{M})$ the computation $\bar{y}_n \xrightarrow{\tau} \dots \xrightarrow{\tau} \bar{y}_1 \xrightarrow{\text{ch}} \bar{y}_0$ exists that satisfies xBy_i for $n \geq i > 0$ and $x'By_0$. We see, this computation of \bar{y} matches the **ch**-transition of \bar{x} as was to be shown. \square

4.2. LTS encoding of symmetric QdCMs.

For finite CMs that are symmetric a simplified version of the encoding can be given. These CMs naturally arise as representations of digital images where points are related via an adjacency relation as discussed in Section 1. Because of the relevance these instances we discuss below a concise version of the encoding of the previous subsection.

Definition 4.6 (Encoding, symmetric case). Let $\mathcal{M} = (X, \mathcal{C}, \mathcal{V})$ be a symmetric CM. Define the labelled transition system $\text{LTS}_{\text{sym}}(\mathcal{M}) = (X, \mathcal{A}, \rightarrow)$ by

- (i) $\mathcal{A} = \text{AP} \cup \{\tau, \text{ch}\}$;
- (ii) the transition relation $\rightarrow \subseteq X \times \mathcal{A} \times X$ contains exactly the following transitions:

$$\begin{aligned} x &\xrightarrow{p} x && \text{for } x \in X, p \in \text{AP} \text{ with } x \in \mathcal{V}(p) \\ x &\xrightarrow{\tau} x' && \text{if } x' \in \mathcal{C}(x) \setminus \{x\} \text{ and } x =_{\mathcal{V}} x' \\ x &\xrightarrow{\text{ch}} x' && \text{if } x' \in \mathcal{C}(x) \text{ and } x \neq_{\mathcal{V}} x' \end{aligned}$$

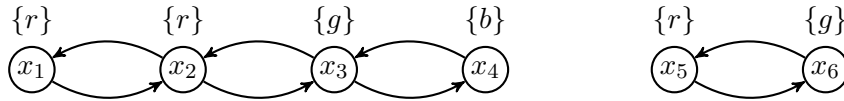


FIGURE 8. A *symmetric* CM.

As an example, consider the symmetric finite QdCM of Figure 8 and its LTS encoding in Figure 9, obtained with the encoding given in Definition 4.6. The minimised model of the symmetric QdCM of Figure 8 is shown in Figure 10. The equivalence classes are the same as in the example of Figure 5 and for the same reasons.

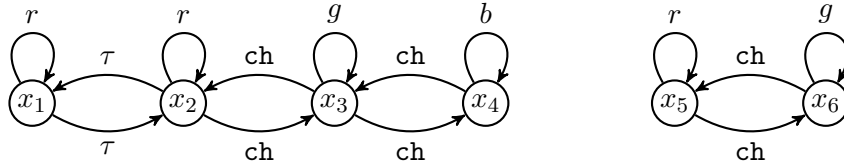
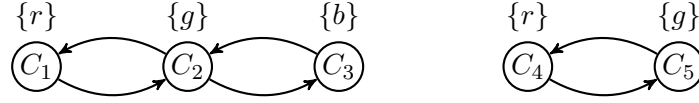


FIGURE 9. LTS resulting from the application of the encoding in Definition 4.6 to the symmetric QdCM of Figure 8.


 FIGURE 10. The minimal *symmetric* CM of that in Fig. 8

Theorem 4.7. *Let $\mathcal{M} = (X, \mathcal{C}, \mathcal{V})$ be a finite and symmetric CM. For $x, y \in X$ it holds that*

$$x \rightleftharpoons_{\text{CoPa}} y \text{ in } \mathcal{M} \text{ iff } x \rightleftharpoons_b y \text{ in } \text{LTS}_{\text{sym}}(\mathcal{M})$$

Proof. We prove the statement $\vec{x} \rightleftharpoons_b \vec{y}$ in $\text{LTS}_{\text{gen}}(\mathcal{M})$ iff $x \rightleftharpoons_b y$ in $\text{LTS}_{\text{sym}}(\mathcal{M})$ for $x, y \in X$. Together with Theorem 4.5, leads to the assertion.

(\Leftarrow) We verify that the relation B given by $B = \{ \langle \vec{x}, \vec{y} \rangle, \langle \vec{x}, \vec{y} \rangle \mid x \rightleftharpoons_b y \}$ is a branching bisimulation relation, where branching bisimilarity of x and y is considered in $\text{LTS}_{\text{sym}}(\mathcal{M})$. Let $x, y \in X$ be such that $x \rightleftharpoons_b y$. Then $\vec{x} B \vec{y}$ and $\vec{x} B \vec{y}$. We first analyze the transitions of \vec{x} in $\text{LTS}_{\text{gen}}(\mathcal{M})$.

- (i) Regarding the transition $\vec{x} \xrightarrow{\text{cv}} x'$ in $\text{LTS}_{\text{gen}}(\mathcal{M})$ we note that $\vec{y} \xrightarrow{\text{cv}} \vec{y}$ and that $\vec{x} B \vec{y}$.
- (ii) If $\vec{x} \xrightarrow{p} \vec{y}$ in $\text{LTS}_{\text{gen}}(\mathcal{M})$ then $x \in \mathcal{V}(p)$ for $p \in \text{AP}$. Also, $x \xrightarrow{p} x$ in $\text{LTS}_{\text{sym}}(\mathcal{M})$. Because $x \rightleftharpoons_b y$, we have $y = y_0 \xrightarrow{\tau} \dots \xrightarrow{\tau} y_{n-1} \xrightarrow{p} y_n$ for some $n > 0$ and $y_0, \dots, y_n \in X$ with $x \rightleftharpoons_b y_0, \dots, y_n$. Because $y_{n-1} \in \mathcal{V}(p)$ it follows from the construction of $\text{LTS}_{\text{sym}}(\mathcal{M})$ that $y_{n-1} = y_n$ and $y_{n-1} \in \mathcal{V}(p)$. As $y_0 \xrightarrow{\tau} \dots \xrightarrow{\tau} y_{n-1}$ it follows from the construction of $\text{LTS}_{\text{sym}}(\mathcal{M})$ as well that $y_0 =_{\mathcal{V}} \dots =_{\mathcal{V}} y_{n-1}$. We conclude that $y = y_0 \in \mathcal{V}(p)$ and therefore $\vec{y} \xrightarrow{p} \vec{y}$ by construction of $\text{LTS}_{\text{gen}}(\mathcal{M})$.
- (iii) If $\vec{x} \xrightarrow{\tau} \vec{x}'$ in $\text{LTS}_{\text{gen}}(\mathcal{M})$ for some $x' \in X$, then it holds that $x = x'$, or $x' \in \mathcal{C}(x) \setminus \{x\}$ and $x =_{\mathcal{V}} x'$. In the first case, i.e. $x = x'$, we have $\vec{x}' = \vec{x} B \vec{y}$. In the second case, $x \xrightarrow{\tau} x'$ in $\text{LTS}_{\text{sym}}(\mathcal{M})$. As $x \rightleftharpoons_b y$, a computation $y = y_0 \xrightarrow{\tau} \dots \xrightarrow{\tau} y_{n-1} \xrightarrow{\tau} y_n$ exists in $\text{LTS}_{\text{sym}}(\mathcal{M})$ with $n \geq 0$, $y_0, \dots, y_{n-1} \rightleftharpoons_b x$, and $y_n \rightleftharpoons_b x'$. We have, without loss of generality, $y_{i+1} \in \mathcal{C}(y_i) \setminus \{y_i\}$ and $y_i =_{\mathcal{V}} y_{i+1}$ for $0 \leq i < n$. Thus, $\vec{y} = \vec{y}_0 \xrightarrow{\tau} \dots \xrightarrow{\tau} \vec{y}_{n-1} \xrightarrow{\tau} \vec{y}_n$ is a computation in $\text{LTS}_{\text{gen}}(\mathcal{M})$, and, by definition of B , it holds that $\vec{x} B \vec{y}_0, \dots, \vec{y}_{n-1}$, and $\vec{x}' B \vec{y}_n$.
- (iv) If $\vec{x} \xrightarrow{\text{ch}} \vec{x}'$ in $\text{LTS}_{\text{gen}}(\mathcal{M})$ for some $x' \in X$, then it holds that $x' \in \mathcal{C}(x)$ and $x \neq_{\mathcal{V}} x'$. So, $x \xrightarrow{\text{ch}} x'$ in $\text{LTS}_{\text{sym}}(\mathcal{M})$. As $x \rightleftharpoons_b y$, a computation $y = y_0 \xrightarrow{\tau} \dots \xrightarrow{\tau} y_{n-1} \xrightarrow{\text{ch}} y_n$ exists in $\text{LTS}_{\text{sym}}(\mathcal{M})$ with $n > 0$, $y_0, \dots, y_{n-1} \rightleftharpoons_b x$, and $y_n \rightleftharpoons_b x'$. We have, without loss of generality, $y_{i+1} \in \mathcal{C}(y_i) \setminus \{y_i\}$ for $0 \leq i < n$ and $y_0 =_{\mathcal{V}} \dots =_{\mathcal{V}} y_{n-1} \neq_{\mathcal{V}} y_n$. Thus, $\vec{y} = \vec{y}_0 \xrightarrow{\tau} \dots \xrightarrow{\tau} \vec{y}_{n-1} \xrightarrow{\text{ch}} \vec{y}_n$ is a computation in $\text{LTS}_{\text{gen}}(\mathcal{M})$, and, by definition of B , it holds that $\vec{x} B \vec{y}_0, \dots, \vec{y}_{n-1}$, and $\vec{x}' B \vec{y}_n$.

Next, we consider transitions of \vec{x} in $\text{LTS}_{\text{gen}}(\mathcal{M})$.

- (i) Regarding the transition $\vec{x} \xrightarrow{\text{dr}} \vec{x}$ in $\text{LTS}_{\text{gen}}(\mathcal{M})$ we note that $\vec{y} \xrightarrow{\text{dr}} \vec{y}$ and $\vec{x} B \vec{y}$.
- (ii) If $\vec{x} \xrightarrow{\tau} \vec{x}'$ in $\text{LTS}_{\text{gen}}(\mathcal{M})$ for some $x' \in X$, then it holds that $x = x'$, or $x \in \mathcal{C}(x') \setminus \{x\}$ and $x =_{\mathcal{V}} x'$. Thus, $x = x'$ or $x \xrightarrow{\tau} x'$ in $\text{LTS}_{\text{sym}}(\mathcal{M})$, by symmetry of \mathcal{M} . In case $x = x'$ we are done since $\vec{x}' = \vec{x} B \vec{y}$. In the other case, we reason as follows. Since $x \rightleftharpoons_b y$, a computation $y = y_0 \xrightarrow{\tau} \dots \xrightarrow{\tau} y_{n-1} \xrightarrow{\tau} y_n$ exists in $\text{LTS}_{\text{sym}}(\mathcal{M})$ with $n \geq 0$, $y_0, \dots, y_{n-1} \rightleftharpoons_b x$, and $y_n \rightleftharpoons_b x'$. From $y_i \xrightarrow{\tau} y_{i+1}$ in $\text{LTS}_{\text{sym}}(\mathcal{M})$, for $0 \leq i < n$, we have, by construction of $\text{LTS}_{\text{sym}}(\mathcal{M})$ (see Definition 4.6), that $y_{i+1} \in \mathcal{C}(y_i)$. In

addition, by symmetry of \mathcal{M} , we get that also $y_i \in \mathcal{C}(y_{i+1})$ holds for $0 \leq i < n$. Thus, by construction of $\text{LTS}_{\text{gen}}(\mathcal{M})$ (see Definition 4.1), we get that $\vec{y}_{i+1} \xrightarrow{\tau} \vec{y}_i$ is a transition of $\text{LTS}_{\text{gen}}(\mathcal{M})$, for $0 \leq i < n$ and then $\vec{y}_n \xrightarrow{\tau} \vec{y}_{n-1} \xrightarrow{\tau} \cdots \xrightarrow{\tau} \vec{y}_0$ is a computation of $\text{LTS}_{\text{gen}}(\mathcal{M})$. By construction of $\text{LTS}_{\text{gen}}(\mathcal{M})$ we also get that $\vec{y} = \vec{y}_0 \xrightarrow{\tau} \cdots \xrightarrow{\tau} \vec{y}_{n-1} \xrightarrow{\tau} \vec{y}_n$ is a computation in $\text{LTS}_{\text{gen}}(\mathcal{M})$. Because $y_0, \dots, y_{n-1} \xleftrightarrow{b} x$ and $y_n \xleftrightarrow{b} x'$, we have $\vec{y}_0, \dots, \vec{y}_{n-1} B \vec{x}$ and $\vec{y}_n B \vec{x}'$ and we are done.

- (iii) If $\vec{x} \xrightarrow{\text{ch}} \vec{x}'$ in $\text{LTS}_{\text{gen}}(\mathcal{M})$ for some $x' \in X$, we proceed in a similar way as in the previous case. It holds that $x \in \mathcal{C}(x')$, $x \neq x'$, and $x \neq_{\gamma} x'$. By symmetry of \mathcal{M} it follows that $x' \in \mathcal{C}(x)$. Thus, $x \xrightarrow{\text{ch}} x'$ in $\text{LTS}_{\text{sym}}(\mathcal{M})$.

Since $x \xleftrightarrow{b} y$, a computation $y = y_0 \xrightarrow{\tau} \cdots \xrightarrow{\tau} y_{n-1} \xrightarrow{\text{ch}} y_n$ exists in $\text{LTS}_{\text{sym}}(\mathcal{M})$ with $n \geq 0$, $y_0, \dots, y_{n-1} \xleftrightarrow{b} x$, and $y_n \xleftrightarrow{b} x'$. From $y_i \xrightarrow{\tau} y_{i+1}$ in $\text{LTS}_{\text{sym}}(\mathcal{M})$, for $0 \leq i < n$, we have, by construction of $\text{LTS}_{\text{sym}}(\mathcal{M})$ (see Definition 4.6), that $y_{i+1} \in \mathcal{C}(y_i)$. In addition, by symmetry of \mathcal{M} , we get that also $y_i \in \mathcal{C}(y_{i+1})$ holds for $0 \leq i < n$. Thus, by construction of $\text{LTS}_{\text{gen}}(\mathcal{M})$ (see Definition 4.1), we get that $\vec{y}_{i+1} \xrightarrow{\tau} \vec{y}_i$ is a transition of $\text{LTS}_{\text{gen}}(\mathcal{M})$, for $0 \leq i < n-1$ as well as $\vec{y}_n \xrightarrow{\text{ch}} \vec{y}_{n-1}$.

Consequently, $\vec{y}_n \xrightarrow{\text{ch}} \vec{y}_{n-1} \xrightarrow{\tau} \cdots \xrightarrow{\tau} \vec{y}_0$ is a computation of $\text{LTS}_{\text{gen}}(\mathcal{M})$. By construction of $\text{LTS}_{\text{gen}}(\mathcal{M})$ we also get that $\vec{y} = \vec{y}_0 \xrightarrow{\tau} \cdots \xrightarrow{\tau} \vec{y}_{n-1} \xrightarrow{\text{ch}} \vec{y}_n$ is a computation in $\text{LTS}_{\text{gen}}(\mathcal{M})$. Because $y_0, \dots, y_{n-1} \xleftrightarrow{b} x$ and $y_n \xleftrightarrow{b} x'$, we have $\vec{y}_0, \dots, \vec{y}_{n-1} B \vec{x}$ and $\vec{y}_n B \vec{x}'$ and we are done.

This finishes the proof from right to left.

(\Rightarrow) We verify that the relation $B = \{ \langle x, y \rangle \mid \vec{x} \xleftrightarrow{b} \vec{y} \text{ in } \text{LTS}_{\text{gen}}(\mathcal{M}) \}$ is a branching bisimulation for $\text{LTS}_{\text{sym}}(\mathcal{M})$. So, let $x, y \in X$ such that $x B y$.

- (i) If $x \xrightarrow{p} x$ in $\text{LTS}_{\text{sym}}(\mathcal{M})$ for $p \in \text{AP}$, then $x \in \mathcal{V}(p)$. Therefore, $\vec{x} \xrightarrow{p} \vec{x}$ in $\text{LTS}_{\text{gen}}(\mathcal{M})$. We have $\vec{x} \xleftrightarrow{b} \vec{y}$ in $\text{LTS}_{\text{gen}}(\mathcal{M})$. So, we can find a matching computation $\vec{y} = \vec{y}_0 \xrightarrow{\tau} \cdots \xrightarrow{\tau} \vec{y}_{n-1} \xrightarrow{p} \vec{y}_n$ for \vec{y} with $n \geq 0$ and $\vec{y}_0, \dots, \vec{y}_n \xleftrightarrow{b} \vec{x}$. Apparently in view of Definition 4.1, $\vec{y}_{n-1} = \vec{y}_n$, and therefore $y_{n-1} \in \mathcal{V}(p)$. As above, an inductive argument shows that $y_{n-1}, \dots, y_0 \in \mathcal{V}(p)$. Hence, $y = y_0 \in \mathcal{V}(p)$. We conclude that $y \xrightarrow{p} y$ in $\text{LTS}_{\text{sym}}(\mathcal{M})$ and this computation for y matches the transition $x \xrightarrow{p} x$.
- (ii) If $x \xrightarrow{\tau} x'$ in $\text{LTS}_{\text{sym}}(\mathcal{M})$ for some $x' \in X$, then $x' \in \mathcal{C}(x)$ and $x =_{\gamma} x'$. Thus, according to Definition 4.1, $\vec{x} \xrightarrow{\tau} \vec{x}'$ is a transition of $\text{LTS}_{\text{gen}}(\mathcal{M})$. Let $\vec{y} = \vec{y}_0 \xrightarrow{\tau} \cdots \xrightarrow{\tau} \vec{y}_{n-1} \xrightarrow{\tau} \vec{y}_n$ for \vec{y} with $n \geq 0$, $\vec{y}_0, \dots, \vec{y}_{n-1} \xleftrightarrow{b} \vec{x}$, and $\vec{y}_n \xleftrightarrow{b} \vec{x}'$ be a matching computation of \vec{y} in $\text{LTS}_{\text{gen}}(\mathcal{M})$. Thus, $y_{i+1} \in \mathcal{C}(y_i)$ and $y_i =_{\gamma} y_{i+1}$ for $0 \leq i < n$. Following Definition 4.6 we conclude that $y = y_0 \xrightarrow{\tau} \cdots \xrightarrow{\tau} y_{n-1} \xrightarrow{\tau} y_n$ is a computation of y in $\text{LTS}_{\text{sym}}(\mathcal{M})$. Moreover, $y_0, \dots, y_{n-1} B x$ and $y_n B x'$. So, this computation of y matches the transition $x \xrightarrow{\tau} x'$ of x .
- (iii) If $x \xrightarrow{\text{ch}} x'$ in $\text{LTS}_{\text{sym}}(\mathcal{M})$ for some $x' \in X$, then $x' \in \mathcal{C}(x)$ and $x \neq_{\gamma} x'$. Therefore $\vec{x} \xrightarrow{\text{ch}} \vec{x}'$ is a transition of \vec{x} in $\text{LTS}_{\text{gen}}(\mathcal{M})$. Let $\vec{y} = \vec{y}_0 \xrightarrow{\tau} \cdots \xrightarrow{\tau} \vec{y}_{n-1} \xrightarrow{\text{ch}} \vec{y}_n$ for \vec{y} with $n \geq 0$, $\vec{y}_0, \dots, \vec{y}_{n-1} \xleftrightarrow{b} \vec{x}$, and $\vec{y}_n \xleftrightarrow{b} \vec{x}'$ be a matching computation of \vec{y} in $\text{LTS}_{\text{gen}}(\mathcal{M})$. Then it holds that $y_{i+1} \in \mathcal{C}(y_i)$ and for $0 \leq i < n$, $y_i =_{\gamma} y_{i+1}$ for $0 \leq i < n-1$, and $y_{n-1} \neq_{\gamma} y_n$. Thus, according to Definition 4.6, we have that $y = y_0 \xrightarrow{\tau} \cdots \xrightarrow{\tau} y_{n-1} \xrightarrow{\text{ch}} y_n$ is a computation of y in $\text{LTS}_{\text{sym}}(\mathcal{M})$. Also we have

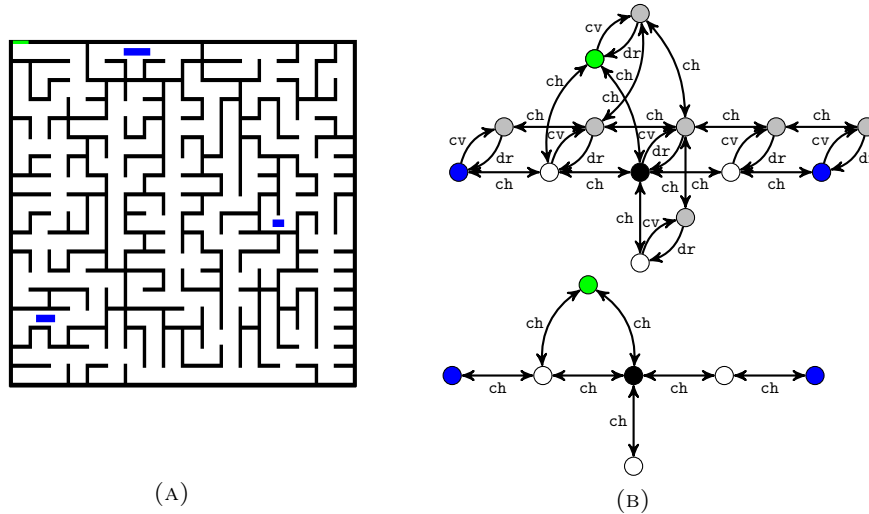


FIGURE 11. An image of a 2D maze, with green exit (upper-left), blue starting points, black walls and white walking areas (Figure 11a), its minimal LTS using the general encoding of Definition 4.1 (Figure 11b - top), and that obtained using the optimised encoding of Definition 4.6 (Figure 11b - bottom). For readability, self-loops labelled by atomic propositions are not shown; the corresponding states are shown in the colour represented by the omitted label; symmetric transition pairs are drawn as doubly-headed arrows.

that $y_0, \dots, y_{n-1} B x$ and $y_n B x'$. Thus, the computation of y is matching the transition $x \xrightarrow{\tau} x'$ of x as was to be shown. □

The 2D maze in Figure 11a, which will also be part of our feasibility study in Section 5, exemplifies the significance of CoPa-minimization on images. Each state of the LTS represents an area of interest in the image: exit (green), walls (black), walking areas (white) and starting points (blue). The three white states, as an example, represent three different kinds of white walking areas: the ones from which neither an exit nor a starting point can be reached (without crossing walls), the ones from which a starting point can be reached (but not the exit), and the ones from which a starting point and the exit can be reached.

5. SPATIAL MODEL CHECKING OF DIGITAL IMAGES VIA MINIMISED MODELS

In this section we present the **VoxMinX** toolchain for spatial model checking of digital images, that exploits the minimisation procedure described in Section 4. We first present a high-level overview of the toolchain, followed by a more detailed discussion in subsequent subsections. We then describe an experimental evaluation showing the feasibility of the proposed toolchain

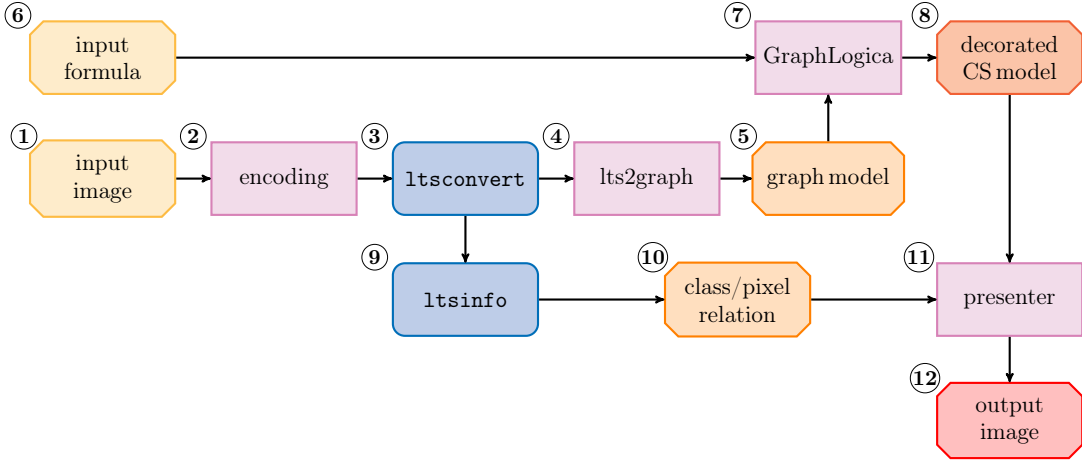


FIGURE 12. **VoxMinX** toolchain for model checking via model minimisation and projection of results onto the original image. Parts 3 and 9 in blue are command line operations of the **mCRL2** toolset. Parts 2, 4, 7 and 11 in purple are developed in Python in the context of the current paper. The orange parts 5, 8 and 10 are intermediate data structures. Parts 1 and 6 in yellow are the input and part 12 in red is the output of the procedure.

and compare its results with that of the spatial model checker **VoxLogicA** for a selected set of benchmark images.

5.1. The **VoxMinX** toolchain.

The major components of the **VoxMinX** toolchain are shown in Figure 12. As input **VoxMinX** takes a digital image (box 1) and a spatial logic specification based on ICRL (box 6). As output, an adaptation of the original image is provided in which the pixels that satisfy the specification are highlighted and the others are shaded. Figure 13 shows an example for the verification of an image of a maze of 4096x4096 pixels against the ICRL formula

$$\phi_1^{maze} = \vec{\zeta} \text{blue}[\text{white}] \wedge \vec{\zeta} \text{green}[\text{white}].$$

Formula ϕ_1^{maze} expresses the fact that a point (pixel) in the image should be white and should be the starting point both of a path passing by white points only reaching a blue point and of a path, passing by white points only, reaching a green point (situated in the upper-left corner of the maze) that represents the exit of the maze. In other words, the formula holds for all white pixels on a path from a blue starting point to the green exit.

The original image of the maze is shown at the left in Figure 13; the adapted image resulting from model checking is shown in the middle. In the latter, the white pixels satisfy the formula, whereas the black pixels do not. At the right in Figure 13 an alternative visualisation of the same results are presented in which the pixels satisfying the formula are highlighted and those that do not satisfy the formula are shaded (i.e. including the shaded

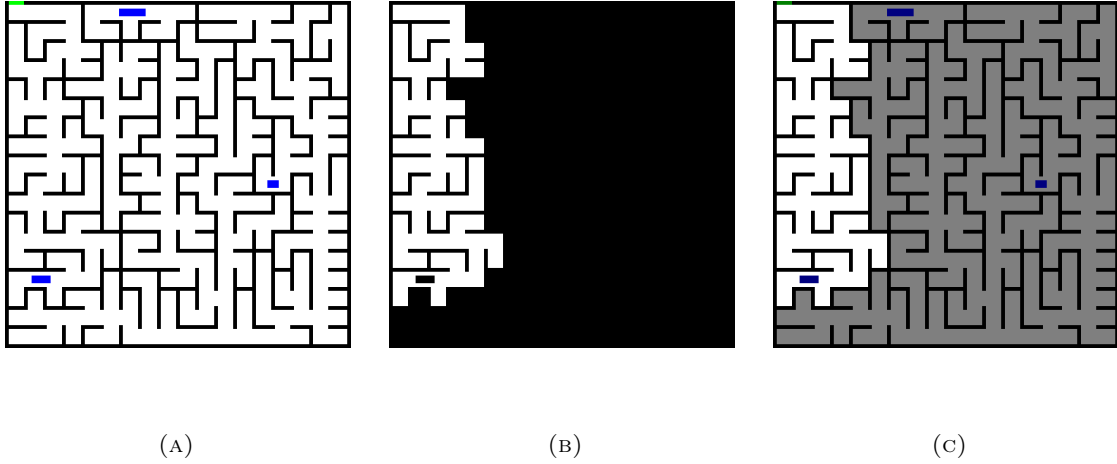


FIGURE 13. Maze example (4096x4096). Figure 13a original image. Figure 13b is showing the model checking results in which pixels satisfying ϕ_1^{maze} are shown in white, others are shown in black. Figure 13c shows an alternative visualisation of the same results where pixels satisfying formula ϕ_1^{maze} are highlighted (white), others are grey-shaded. The green exit is situated in the top left corner of the maze in Figure 13a.

black, green and blue ones). These are only two examples of how the results can be presented. Depending on the application area, other presentations could be more common or adequate. For example, in medical imaging, regions of interest (ROI) in images are often shown as a semi-transparent overlay, in a colour of choice, overlapping the original image. An example is shown in Figure 1, where the pixels satisfying the logic specification that identifies tumour and oedema tissue, are shown in semi-transparent green, whereas the pixels in red are part of the ground truth provided by human experts. Note that the green and red overlays are mostly overlapping and that the differences between the two tumour segmentations are shown as (a small number of) bright red and bright green pixels. The latter feature greatly facilitates the assessment of the quality of the segmentation obtained by spatial model checking with respect to the ground truth. Such alternative visual presentations can be easily accommodated by adjusting the back-end software of the toolchain or via the user interface settings of the visualisation tool that has been developed for VoxLogicA [Str25].

In Figure 14 a more colourful and complex image is shown of a scene of the well-known video game Pac-Man⁴ that is checked against the nested ICRL formula

$$\vec{\zeta}(\vec{\zeta} \text{ blue}[\text{white}]) [-(\text{black} \vee \text{blue})] \quad (5.1)$$

This formula holds for all the so-called Ghost Monster figures in this picture. Observe that the eyes of the ghosts are composed of a blue and a white part and that each Ghost Monster has at least one eye in which the blue part does not touch the black background

⁴Pac-Man Official Website – History: <https://pacman.com/en/history/>. Accessed on September 2, 2025.

but does touch the white part of the eye instead. Such a spatial configuration only occurs in the ghosts, and therefore the formula uniquely identifies them. The original image of the Pac-Man scene is shown on the left; the image in the middle is showing model checking results where pixels satisfying the formula are shown in white and the others in black. An alternative visualisation is shown on the right, where the highlighted pixels (identifying the ghosts) satisfy the formula, and the shaded pixels do not.

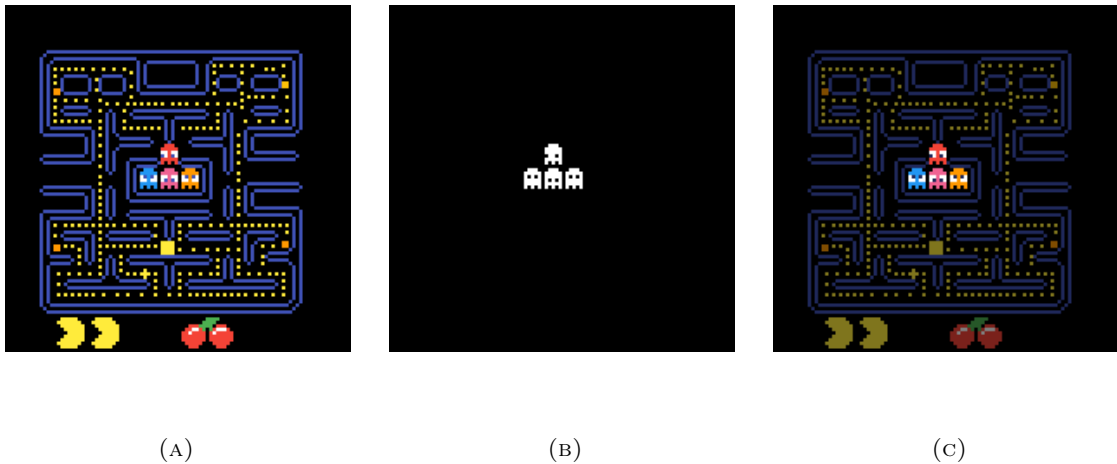


FIGURE 14. Pacman example (200x200 pixels). Figure 14a original image. Figure 14b shows pixels satisfying formula `ghosts` in white, others are shown in black. Figure 14c pixels satisfying formula `ghosts` as highlighted colours, others are shown in shaded colours.

Next, let us have a closer look at the other parts of the toolchain in Figure 12. First the input image (box 1) is converted into a QdCM representation and fed through an encoder (box 2), which converts the image into an LTS, implementing the encoding defined in Definition 4.6. This LTS has one state for each pixel of the image with a self-loop recording the colour of the pixel in its label. The LTS is subsequently minimised with respect to branching bisimilarity using an existing minimisation tool available from the `mCRL2` tool suite [BGK⁺19] (box 3). Care is taken that the resulting equivalence classes, represented by the states of the minimal LTS, remain associated to their respective set of pixels in the original image. The minimal LTS is then transformed into an annotated closure space model representing the minimal QdCM modulo CoPa-bisimilarity (box 5). This transformation is the implementation of what is established by Theorem 3.5. The closure space model (box 5) and the input formula (box 6) are provided as input to the `GraphLogica` model checker (box 7, discussed below). The model checking result (box 8) is an annotated version of the input closure space model in which the points that satisfy the formula are indicated by a specific label. These points are representatives of equivalence classes of pixels present in the input image. This outcome of the model checker (box 8) is then combined with the information linking the equivalences

classes to the sets of pixels they represent (box 10) by the presenter (box 11) and used to produce the adapted input image as output (box 12). We refer the reader interested in further details on each of the steps in the toolchain, and the particular file formats involved, to the small running example presented in Appendix A.

In the previous section, in Figure 11a we have already seen the example of the maze and the minimal models that are obtained applying the general encoding (see Definition 4.1) and the optimised encoding (see Definition 4.6) followed by branching bisimulation minimisation. Let us here consider a more complex example using *VoxMinX*. Figure 15 shows the minimal LTS, obtained after an optimised encoding, for the scene of the Pac-Man game shown in Figure 14a. This minimal model has 35 states, each representing an equivalence class (of pixels) modulo ICRL. It is not difficult to recognise some groups of states representing specific parts of the image. For example, at the left one observes a group of two white, two red and a green state (states 1, 5, 9, 33, 34). This group represents the two cherries at the bottom of the original Pac-Man image. The single black node in the middle (state 4) represents all pixels of the black background. Note that there is only one such state because *VoxMinX*, like *VoxLogicA*, constructs a regular graph model from a digital image based on an 8-adjacency relationship⁵ between pixels, so also those pixels touching diagonally are considered adjacent in the graph. Therefore all black pixels are adjacent. The four groups of states at the top of the figure represent the four ghosts: On the left, states 10, 24, 29, 30, 31, and 32 represent the red ghost; next of that group on the right the states 3, 13, and 14 represent the cyan ghost; next of the latter group the states 2, 6, and 8 represent the pink ghost, and on the right the states 7, 11, and 25 represent the orange ghost. Note that each ghost has indeed a blue state (representing blue pixels of the eye) that has no transition to the black state (state 4). We used this observation to find a formula to identify the ghosts. With the red ghost three blue states are associated. Two of them have a transition to the black state (state 4) but they represent different equivalence classes of pixels. State 30 represents blue pixels that are not part of an eye but are actually part of the blue stripes marking the sides of paths in the Pac-Man game that happen to touch the red part of the ghost (situated on top of its head). State 29, instead, represents pixels of the only eye of the red ghost (its right eye) that has a blue part touching the black background. At the bottom of Figure 15 we can observe the states 12, 21 and 22, that represent a pale orange cookie, coloured slightly different from the other three orange cookies, in the top-right of the original image. That specific cookie does touch a blue pixel (belonging to the border of a path) that, in turn, touches a yellow pellet (diagonally). The single yellow state (state 0) represents both the pixels of the yellow Pac-Man items at the bottom of the image, and the pixels of most of the yellow pellets. Note that these objects are all surrounded by black pixels belonging to the background.

⁵In digital image processing the basic relationships between pixels are the 4-adjacency and the 8-adjacency relationship. The former considers four neighbours of each pixel in the adjacency relationship, namely its left and right neighbours and its neighbours directly above and below it. The latter considers also the four diagonal neighbours of a pixel. This holds for all pixels except for those at the border of the image that have a reduced number of neighbours depending on their position.

the **VoxLogicA** model checker is not dealing with general graphs but specialised for images. We briefly describe some of the main features of these tools below.

The GraphLogicA model checker. In **VoxMinX** we employ the spatial model checker **GraphLogicA**. It implements a basic spatial model checking algorithm for the finitary fragment of ICRL on general graphs, based on the analysis of connected components for CMs which are not necessarily symmetric. The reachability operators of ICRL are provided explicitly by the specification language **GrQL** of **GraphLogicA** (**GrQL** is short for Graph Query Language). In **GrQL**, one or more logical formulas can be specified that are to be checked against the input model. When multiple formulas are given, they are checked one after the other in the same model checking session. Moreover, **GraphLogicA** provides the implementation of the encodings presented in Section 4.

The mCRL2 toolset. The **mCRL2** toolset [GM14, BGK⁺19] is a collection of tools for the analysis of models of distributed and concurrent systems. Its process language is based on the Algebra of Communicating Processes [BW90], its property specification language is based on the modal μ -calculus [BS07]. The toolset includes a temporal model checker to formally verify and analyse models of complex software and protocols. It also includes operations for the minimisation of models based on various types of bisimilarity equivalences, in particular, the branching bisimilarity minimisation using the optimized algorithm proposed in [GJKW17].

The VoxLogicA model checker. In [BCLM19b, BCM25] the **VoxLogicA** model checker an implementation of the model checking algorithm is presented. **VoxLogicA** is specialised for digital images. In particular, it employs efficient procedures⁶ for the analysis of connected components. The tool **VoxLogicA** implements, among others, a spatial model checking procedure for a logical operator for conditional reachability, included in **ImgQL**, the specification language of **VoxLogicA**.

In order to measure the model checking speed-up of the **VoxMinX** toolchain, with respect to direct spatial model checking of the full original images, we use **GraphLogicA** for checking the minimal model, and **VoxLogicA** to check the full model⁷.

The tests have been performed on a MacBook Pro equipped with an Apple M2 Pro processor and 32GB of RAM running macOS Sequoia 15.7. The **mCRL2** toolset version `mcr2-202507.0.66927898fc_arm64` was used. In this version **mCRL2** uses a non-recursive procedure to find strongly connected components that does not require a large stack. Full data, source code and tools needed to reproduce the maze and monoscope experiments can be found in the Zenodo repository [CM26].⁸

For the experimental evaluation we have used a benchmark consisting of three families of images: a family of maze images (see Figure 11a), a family of monoscope image (see Figure 16), and a family of images of a snapshot of the Pac-Man game (see Figure 14a). Each family consists of a benchmark image that has been rescaled at various resolutions. The

⁶In particular, this implementation exploits very efficient algorithms from the Insight Tool Kit (ITK) via the **SimpleITK** glue, see <https://itk.org> and <http://www.simpleitk.org> library [LCIB13, MLI⁺14] specially designed for (medical) digital image processing.

⁷We underline again that **VoxLogicA** is inherently much faster than **GraphLogicA** as it is specialised for images, exploiting state-of-the-art imaging libraries and automatic parallelisation. This poses a further challenge to the speed-up via minimisation and is the reason why we use **VoxLogicA** instead of **GraphLogicA** for the full model.

⁸The results are currently available at a public repository on GitHub at: <https://github.com/VoxLogicA-Project/VoxMinX-Validation>

The Zenodo repository will be produced for the final version of the paper based on the GitHub repository.



FIGURE 16. Monoscope test pattern Philips PM5544

names of the images in each family are composed of their name (*maze*, *mono*, *pm*) followed by a numeric indication of the vertical resolution of each image. The *maze* and the *Pac-Man* images are square, therefore their horizontal resolution coincides with their vertical one. For example, *maze-1024* is a *png* image of the maze of 1024 pixels wide and 1024 pixels high. The monoscope image has a 16:9 ratio, thus, e.g., the horizontal resolution of *mono-1080* is 1920 pixels.

For the experiment with the *maze image*, the property specification consists of the three reachability formulas that identify

- (1) the white points from which both a blue point and a green point can be reached (in other words, the white paths connecting blue points to the green exit)

$$\varphi_1^{maze} = \vec{\zeta} \text{ green}[white] \wedge \vec{\zeta} \text{ blue}[white]$$

- (2) the blue points from which there is *no* white path to the green exit

$$\varphi_2^{maze} = \text{blue} \wedge \neg \vec{\zeta} (\vec{\zeta} \text{ green}[white])[blue]$$

- (3) the blue points from which, instead, an exit *can* be reached

$$\varphi_3^{maze} = \vec{\zeta} (\vec{\zeta} \text{ green}[white] \wedge \vec{\zeta} \text{ blue}[white])[blue]$$

Note that it holds that $\varphi_3^{maze} = \vec{\zeta} \varphi_1^{maze}[blue]$.

For the *monoscope image*, the property specification is slightly artificial as it has been designed to be increasingly demanding in terms of computation time (caused by the nesting of sub-formulas). A single property φ^{mono} is used in the experiments, that characterises the points from which very specific paths start, crossing a number of different colours in a specific order, using 16 nested reachability constraints, of the form

$$\varphi^{mono} = \vec{\zeta} (\vec{\zeta} (\vec{\zeta} (\dots)[green])[cyan])[yellow]$$

For the *Pac-Man scene*, the logic specification illustrates how several objects of interest can be identified in the *Pac-Man scene*. These are the eyes of the ghosts, the cherries, the pellets, and the ghosts themselves, exploiting the various colours of the pixels and their relationship with other pixels. For the *Pac-Man scene*, the property specification consists of the reachability formulas φ_1^{pm} to φ_4^{pm} below.

- (1) The eyes of the ghosts can be uniquely identified by white pixels through which blue pixels can be reached. This can be expressed via the formula

$$\varphi_1^{pm} = \vec{\zeta} \text{blue}[\text{white}]$$

Formula φ_1^{pm} is also discussed in Equation (5.1) above.

- (2) The cherries are uniquely identified by red, white, or green pixels through which green pixels can be reached. This can be expressed via formula

$$\varphi_2^{pm} = \vec{\zeta} \text{green}[(\text{red} \vee \text{white} \vee \text{green})]$$

- (3) Pellets are the four small orange squares.⁹ They are not the only orange pixels, because there is also an orange ghost. To distinguish the orange pixels of pellets, we require that they are not those via which one can reach the eyes of the orange ghost. This can be expressed via formula

$$\varphi_3^{pm} = \text{orange} \wedge \neg \vec{\zeta} \varphi_1^{pm}[\text{orange}]$$

- (4) The ghosts themselves are uniquely identified by the colour of their pixels (one red, one cyan, one orange, and one pink, which is not black or blue) and the fact that they all have at least one white with blue eye that is not touching the black background. This can be expressed via the formula

$$\varphi_4^{pm} = \vec{\zeta} \varphi_1^{pm}[(\neg(\text{black} \vee \text{blue}))]$$

5.3. Performance Results. Table 1, Table 2, and Table 3 report the **VoxMinX** results for each test image, for the logical properties specified earlier. We have run all the phases of our experiment for each image, also in the cases that produce the same minimal models, for simplicity of the set-up.

Each table shows the results for a specific image and its rescaled versions. Table 1 shows the results for the maze. The first column shows the name of the image, where the number attached to the name indicates the vertical resolution of the image in terms of the number of pixels. The second and third column show the time in seconds needed to perform the encoding, the former shows the pure computation time, whereas the latter includes the time for writing the result to file (i.e. including IO). The fourth, fifth, and sixth columns provide the number of states, transitions, and the size of the full model of the image (i.e. before minimisation), respectively. Columns seven to eleven provide, respectively, the minimisation time, without and with IO, the number of states of the minimal model, the number of transitions and the time to translate the results back to the original image. The last three columns of the table provide the pure model checking time of the full model (performed with **VoxLogicA**), the model checking time of the minimal model (performed with **GraphLogicA**), and the speed-up (gain) in model checking time obtained when using the minimal model compared to model checking the full model, respectively. All times are in seconds, rounded to two decimals.

⁹One of the pellets in Figure 14a has a somewhat fainter orange colour. We will abstract from this here and consider them all the orange colour.

name	Encoding		Full model			Minimisation					Model checking		
	time	t.w.IO	states	trans.	aut file size	time	t.w.IO	stat.	trans.	t.back	t.full	t.min	gain
maze-128	0.18	0.21	16.00 K	142.50 K	2.47 MB	0.00	0.11	7	21	0.20	0.72	0.22	3.33
maze-256	0.18	0.24	64.00 K	573.00 K	10.35 MB	0.02	0.38	7	21	0.24	0.71	0.22	3.30
maze-512	0.18	0.39	256.00 K	2.24 M	44.55 MB	0.11	1.66	7	21	0.42	0.72	0.22	3.33
maze-1024	0.19	0.86	1.00 M	8.99 M	184.34 MB	0.48	7.71	7	21	1.13	0.75	0.22	3.48
maze-2048	0.24	2.88	4.00 M	35.98 M	793.73 MB	2.32	33.98	7	21	4.59	0.94	0.22	4.35
maze-4096	0.45	10.69	16.00 M	143.95 M	3.27 GB	9.89	145.63	7	21	19.79	2.46	0.22	11.03
maze-8192	0.97	42.35	64.00 M	575.91 M	13.63 GB	51.90	599.01	7	21	80.82	3.85	0.22	17.77

TABLE 1. Results for the maze case study. All times are in seconds, rounded to two decimals. From left to right: encoding time for the image (png file) into automata format (aut file) conversion, without and with I/O; number of states, transitions, and aut file size of full model; minimisation time, without and with I/O; number of states and transitions of minimal LTS; time to convert the minimal (aut file) model into a QdCM (json file); time for model checking the full model with `VoxLogicA`, and the minimal model with `GraphLogicA`; model checking speed-up.

The obtained speed-up (last column) is noteworthy, ranging from 3 to more than 17 times faster model checking when using minimised models, especially for the larger images, as shown in the last lines in the right-most column (gain) in the Table 1. Note that the minimal model has the same number of states and transitions for each of the scaled images. This is as expected, as the size of each element in the images does not matter for CoPa-bisimilarity, but only the (conditional) reachability between elements of different colour as established by the spatial logic. The processing times to produce the encoding of the full model increase with the size of the input image. Also the generation of the intermediate result files in the tool chain is rather large and requires time to be produced. This is an aspect that can be overcome in a subsequent implementation of the toolchain in which intermediate results are stored internally. The current experimental toolchain was built with the aim to first get insight in the potential gains of the model checking times. Note, however, that the experimental version of `VoxMinX` is nevertheless already able to handle images of considerable size, i.e. 64M pixels. The time to translate the model checking results obtained from the minimal model back to the full image is not constant, but varies with the size of the input image. This is because this translation has to take the equivalence classes of pixels into account, which tend to be larger in larger images, thus requiring more processing time.

Similar observations can be made for the results for the more involving monoscope image shown in Table 2, that has the same structure as Table 1. In this case, a single property is evaluated that is characterised by a deep nesting of conditional reachability operators. For the largest of this set of images the speed-up is more than 25 times that of the model checking time for the full (i.e. non-minimised) version. This more complex image leads to minimal models with a considerable number of states, ranging from 155 for the smallest image, to 945 for the largest image. The reason that for this image the minimal models are not all identical is that downscaling of the image reduces the number of details that can be distinguished (e.g. some thin lines simply disappear). This leads to a smaller number of equivalence classes for the smaller images. It also explains why for the largest model, with

name	Encoding		Full model			Minimisation					Model checking		
	time	t.w.IO	states	trans.	aut file size	time	t.w.IO	stat.	trans.	t.back	t.full	t.min	gain
mono-130	0.18	0.21	30.47 K	272.05 K	4.83 MB	0.01	0.22	155	899	0.22	0.76	0.25	3.01
mono-260	0.26	0.28	121.88 K	1.07 M	20.27 MB	0.05	0.74	315	1841	0.40	1.06	0.28	3.78
mono-540	0.19	0.54	506.25 K	4.44 M	90.33 MB	0.20	3.31	460	2766	0.69	0.87	0.28	3.05
mono-1080	0.21	1.49	1.98 M	17.78 M	384.28 MB	0.97	14.57	945	6965	2.31	1.26	0.33	3.84
mono-2160	0.28	5.36	7.91 M	71.16 M	1.55 GB	3.79	63.66	945	6965	9.50	2.67	0.33	8.15
mono-4320	0.58	21.13	31.64 M	284.70 M	6.65 GB	15.71	258.92	945	6965	42.15	8.28	0.33	25.21

TABLE 2. Results for the monoscope case study. All times are in seconds, rounded to two decimals. From left to right: encoding time for the image (png file) into automata format (aut file) conversion, without and with I/O; number of states, transitions, and aut file size of full model; minimisation time, without and with I/O; number of states and transitions of minimal LTS; time to convert the minimal (aut file) model into a QdCM (json file); time for model checking the full model with `VoxLogicA`, and the minimal model with `GraphLogicA`; model checking speed-up.

more details, the model checking time of the full model is significantly higher, while there is an only limited increase in the model checking time of the minimal model.

For what concerns the results for the Pac-Man scene, shown in Table 3, rescaling of the image did not change the structure of the image. Therefore, in this case, the number of states (and transitions) of the minimal model are the same for all cases, i.e. 35 states and 155 transitions. The speed-up that is obtained is somewhat smaller compared to that found for the other two cases. However, it is still 7 times faster to perform model checking on the minimal model, compared to model checking the full model.

Regarding this experimental evaluation, it is noted that the `VoxLogicA` model checker is highly optimised for images, whereas the `GraphLogicA` variant is working on general graphs and more of an experimental, and less optimised, nature. So the results on speed-up of the model checking times are actually underestimated. Furthermore, once a minimal model has been generated, it can be used for many model checking sessions, which is increasing the advantage considering computation time.

The plots in Figure 17 provide a visual presentation of some of the numbers in the previous tables. Figure 17a shows how the speed-up is related to the size of an image, for the maze (blue), the monoscope (red), and the Pac-Man scene (brown), respectively. For the maze, the increase in speed-up and the increase in model checking time of the full model appears not to be linear. Presumably, full model checking is relatively fast for the larger models, probably due to some possibilities to reuse partial results in the optimisation of the model checking procedure of `VoxLogicA`. Figure 17b shows how the full model checking time relates to the size of the images. It shows a similar pattern as in Figure 17a. Finally, in Figure 17c it is shown how the minimisation time relates to the size of the images. This seems to follow essentially a linear pattern for each case.

In this section we have studied spatial model checking for digital images using model minimisation based on CoPa-bisimilarity. We have used `VoxMinX` on several types of images,

name	Encoding		Full model			Minimisation					Model checking		
	time	t.w.IO	states	trans.	aut file size	time	t.w.IO	stat.	trans.	t.back	t.full	t.min	gain
pm-200	0.18	0.22	39.06 K	349.22 K	6.29 MB	0.02	0.26	35	155	0.22	0.71	0.22	3.25
pm-400	0.18	0.30	156.25 K	1.37 M	26.56 MB	0.08	0.95	35	155	0.33	0.73	0.22	3.30
pm-600	0.18	0.46	351.56 K	3.08 M	61.97 MB	0.17	2.40	35	155	0.51	0.75	0.22	3.37
pm-800	0.18	0.63	625.00 K	5.48 M	111.49 MB	0.31	4.57	35	155	0.79	0.75	0.22	3.39
pm-1000	0.19	0.82	976.56 K	8.57 M	175.13 MB	0.46	7.21	35	155	1.12	0.77	0.22	3.49
pm-2000	0.23	2.68	3.81 M	34.31 M	756.49 MB	1.92	31.48	35	155	4.46	0.96	0.22	4.34
pm-4000	0.38	10.30	15.26 M	137.28 M	3.11 GB	7.93	134.44	35	155	18.83	1.62	0.22	7.34

TABLE 3. Results for the Pac-Man case study. All times are in seconds, rounded to two decimals. From left to right: encoding time for the image (png file) into automata format (aut file) conversion, without and with I/O; number of states, transitions, and aut file size of full model; minimisation time, without and with I/O; number of states and transitions of minimal LTS; time to convert the minimal (aut file) model into a QdCM (json file); time for model checking the full model with VoxLogicA, and the minimal model with GraphLogicA; model checking speed-up.

ranging from the synthetic 2D maze example to images from the ‘real world’ such as the Pac-Man scene and the monoscope example. The analysis shows promising results for what concerns the speed-up in model checking time that can be obtained using minimal models. Moreover, it also shows that the approach is applicable to images of a size that is easily found in various application areas, for example, the largest maze consists of 64M pixels. At the same time, it also shows that a further integration of the tools that the VoxMinX toolchain is composed of would be very beneficial to reduce resources needed for the various transformations. We envision that such improvements would facilitate the wider applicability of the method. In particular, we are interested in its application in the domain of medical imaging. VoxLogicA has already been applied to that area, see for example [BCM25], where the contouring of brain tumours and the segmentation of white and grey matter of the brain were addressed. However, the method could find its way to other medical applications and many other domains in which spatial analysis is of interest [CLM25, BBC⁺26, ACLM26, BCLM26].

6. CONCLUSIONS AND FUTURE WORK

Traditional model checking is a widely used verification technique for ensuring that a model of system behaviour conforms to a logical specification of desired properties. *Spatial* model checking, where a model of space is checked against a spatial logic formula, expressing *spatial* properties, has proven a valuable verification technique. It has been successfully applied in various domains, in particular in medical image analysis. One way to improve the performance of spatial model checking is by model reduction. In this paper we have shown that this can be obtained exploiting the logical characterisation of CoPa-bisimilarity

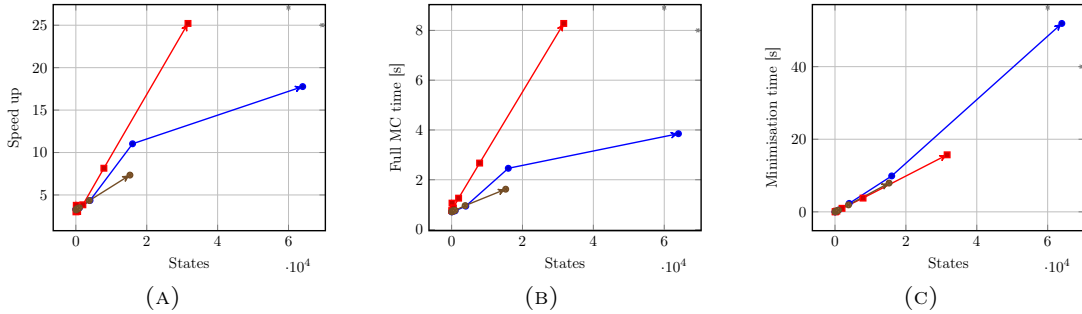


FIGURE 17. **VoxMinX**: Model size in number of states vs. speed-up factor for the maze (blue), the monoscope (red) and the Pac-Man (brown) examples (17a). For the same models: number of states vs. model checking of full model with **VoxLogicA** (17b) and number of states vs. minimisation time without IO (17c).

by the ICRL logic. (In-)finitary Compatible Reachability Logic includes conjunction and two conditional reachability modalities: one forward and one backward modality.

A practical and feasible minimisation method has been proposed for CoPa-bisimilarity for finite closure models. The latter are a convenient theoretical framework for model checking spatial logics. The method relies on an encoding of (finite) closure models into suitable LTSs such that an existing efficient algorithm for branching bisimilarity can be used to obtain a minimal model. The encoding has been proven correct, in the sense that two points in the closure models are CoPa-bisimilar if and only if the states they are mapped to by the encoding are branching bisimilar in the corresponding LTS. The correctness proof exploits induction based on the novel notion of depth of a state in an LTS.

An implementation of the encoding has been developed for the special case of symmetric closure models representing digital images. The implementation is part of a toolchain, **VoxMinX**, that uses a branching bisimilarity minimisation procedure from the **mCRL2** toolset for the minimisation of the LTS encoding the original image. It also translates the spatial model checking results for the minimal model back to the pixels in the original image that was taken as input. Doing so, model checking results can be directly made visible on the input image itself. For example, **VoxMinX** can highlight the pixels that satisfy the spatial property of interest while showing the other pixels in a shaded way. This provides the user with an immediate and informative visual feedback of the results of spatial model checking on images.

A feasibility study has been performed for **VoxMinX**. This study uses a benchmark of images and formulas and provides insight in the potential of the minimisation method for its use in the analysis of, possibly large, 2D images. The benchmark consists of three series of representative images. Each image has been evaluated at six or seven different resolutions to be able to evaluate the performance for increasing sizes of the images. For each set of images, the results confirm that a very promising speed-up of spatial model checking can be obtained for single formulas, also for images with a huge, but realistic, size. This insight is particularly relevant for the envisioned use of spatial model checking in the medical domain.

Of course, minimisation pays off more when multiple formulas are checked on the same model, which is common in formal verification. In such a scenario, the multiple model

checking time for the full model can in general be expected to be substantially longer than the sum of the conversion, minimisation, backwards conversion, and multiple model checking time of the minimal model, even for the current prototype. The advantage increases, of course, when multiple properties are checked on a single minimised model. Furthermore, bisimulation-based minimisation of images may also serve as a particular form of compression of large images. Such compression preserves all the spatial properties of the original image that can be expressed by the spatial logic, but requires, in general, much less space to be stored.

Ongoing work, also taking into account the results presented in [Zev22], is devoted to translating spatial-logic properties to the language of `mCRL2` in order to use its state-of-the-art model checking techniques to verify spatial properties of directed graphs, in order to leverage the obtained speed-up even further. Future work aims at further optimisations of the representations of the models and an integration of the components present in the `VoxMinX` toolchain. The basic ingredients for such a mapping, i.e. the sets of states in the equivalence classes of the bisimulation, are readily available using the `mCRL2` tool suite [BGK⁺19].

ACKNOWLEDGMENT

Research partially supported by bilateral project between CNR (Italy) and SRNSFG (Georgia) “Model Checking for Polyhedral Logic” (#CNR-22-010); European Union – Next GenerationEU – National Recovery and Resilience Plan (NRRP), Investment 1.5 Ecosystems of Innovation, Project “Tuscany Health Ecosystem” (THE), CUP: B83C22003930001; European Union – Next-GenerationEU – National Recovery and Resilience Plan (NRRP) – MISSION 4 COMPONENT 2, INVESTMENT N. 1.1, CALL PRIN 2022 D.D. 104 02-02-2022 – (Stendhal) CUP N. B53D23012850006; MUR project PRIN 2020TL3X8X “T-LADIES”; CNR project “Formal Methods in Software Engineering 2.0”, CUP B53C24000720005; Shota Rustaveli National Science Foundation of Georgia grant #FR-22-6700.

REFERENCES

- [ABGP⁺06] B. Aubert-Broche, M. Griffin, G.B. Pike, A.C. Evans, and D.L. Collins. Twenty new digital brain phantoms for creation of validation image data bases. *IEEE Transactions on Medical Imaging*, 25(11):1410–1416, 2006.
- [ACLM26] Yuri Andriaccio, Vincenzo Ciancia, Diego Latella, and Mieke Massink. Practical polyhedral model checking. In Maurice H. ter Beek, Stefania Gnesi, Anne E. Haxthausen, and Laura Semini, editors, *Journeys Between Formal Methods and the Railway Industry: Essays Dedicated to Alessandro Fantechi on the Occasion of His 70th Birthday*, pages 138–159, Cham, 2026. Springer Nature Switzerland.
- [Aie02] M. Aiello. *Spatial Reasoning: Theory and Practice*. PhD thesis, Institute of Logic, Language and Computation, University of Amsterdam, 2002.
- [Aie03] M. Aiello. The topo-approach to spatial representation and reasoning. *AIIA NOTIZIE*, (4), 2003.
- [APB07] Marco Aiello, Ian Pratt-Hartmann, and Johan van Benthem, editors. *Handbook of Spatial Logics*. Springer, 2007.
- [BBC⁺20] Fabrizio Banci Buonamici, Gina Belmonte, Vincenzo Ciancia, Diego Latella, and Mieke Massink. Spatial logics and model checking for medical imaging. *Int. J. Softw. Tools Technol. Transf.*, 22(2):195–217, 2020.
- [BBC⁺21] Gina Belmonte, Giovanna Broccia, Vincenzo Ciancia, Diego Latella, and Mieke Massink. Feasibility of spatial model checking for nevus segmentation. In Simon Bliudze, Stefania Gnesi, Nico Plat, and Laura Semini, editors, *9th IEEE/ACM International Conference on Formal Methods*

- in *Software Engineering, FormaliSE@ICSE 2021, Madrid, Spain, May 17-21, 2021*, pages 1–12. IEEE, 2021.
- [BBC⁺26] Nick Bezhanishvili, Laura Bussi, Vincenzo Ciancia, David Gabelaia, Mamuka Jibladze, Diego Latella, Mieke Massink, and Erik P. de Vink. Weak simplicial bisimilarity and minimisation for polyhedral model checking. *Log. Methods Comput. Sci.*, 22(1), 2026.
- [BCG⁺22] Nick Bezhanishvili, Vincenzo Ciancia, David Gabelaia, Gianluca Grilletti, Diego Latella, and Mieke Massink. Geometric Model Checking of Continuous Space. *Logical Methods in Computer Science*, Volume 18, Issue 4, November 2022.
- [BCG⁺24] Nick Bezhanishvili, Vincenzo Ciancia, David Gabelaia, Mamuka Jibladze, Diego Latella, Mieke Massink, and Erik P. de Vink. Weak simplicial bisimilarity for polyhedral models and SLCS η . In Valentina Castiglioni and Adrian Francalanza, editors, *Formal Techniques for Distributed Objects, Components, and Systems - 44th IFIP WG 6.1 International Conference, FORTE 2024, Groningen, The Netherlands, June 17-21, 2024, Proceedings*, volume 14678 of *Lecture Notes in Computer Science*, pages 20–38. Springer, 2024.
- [BCLM19a] Gina Belmonte, Vincenzo Ciancia, Diego Latella, and Mieke Massink. Innovating medical image analysis via spatial logics. In Maurice H. ter Beek, Alessandro Fantechi, and Laura Semini, editors, *From Software Engineering to Formal Methods and Tools, and Back - Essays Dedicated to Stefania Gnesi on the Occasion of Her 65th Birthday*, volume 11865 of *Lecture Notes in Computer Science*, pages 85–109. Springer, 2019.
- [BCLM19b] Gina Belmonte, Vincenzo Ciancia, Diego Latella, and Mieke Massink. Voxlogica: A spatial model checker for declarative image analysis. In Tomás Vojnar and Lijun Zhang, editors, *Tools and Algorithms for the Construction and Analysis of Systems - 25th International Conference, TACAS 2019, Proceedings, Part I*, volume 11427 of *Lecture Notes in Computer Science*, pages 281–298. Springer, 2019.
- [BCLM26] Gina Belmonte, Vincenzo Ciancia, Diego Latella, and Mieke Massink. Model checking in space with applications to medical image analysis - invited abstract. In Elvira Albert and Corina S. Pasareanu, editors, *Fundamental Approaches to Software Engineering - 29th International Conference, FASE 2026, Turin, Italy, April 11-16, 2026, Proceedings*, Lecture Notes in Computer Science, pages 3–18. Springer, 2026.
- [BCM25] Gina Belmonte, Vincenzo Ciancia, and Mieke Massink. Symbolic and hybrid AI for brain tissue segmentation using spatial model checking. *Artif. Intell. Medicine*, 167:1–20, 2025.
- [BGK⁺19] Olav Bunte, Jan Friso Groote, Jeroen J. A. Keiren, Maurice Laveaux, Thomas Neele, Erik P. de Vink, Wieger Wesselink, Anton Wijs, and Tim A. C. Willemse. The mCRL2 toolset for analysing concurrent systems - improvements in expressivity and usability. In Tomás Vojnar and Lijun Zhang, editors, *Tools and Algorithms for the Construction and Analysis of Systems - 25th International Conference, TACAS 2019, Proceedings, Part II*, volume 11428 of *Lecture Notes in Computer Science*, pages 21–39. Springer, 2019.
- [BS07] Julian C. Bradfield and Colin Stirling. Modal mu-calculi. In Patrick Blackburn, Johan van Benthem, and Frank Wolter, editors, *Handbook of Modal Logic*, Studies in logic and practical reasoning, pages 721–756. North-Holland, 2007.
- [BW90] J.C.M. Baeten and W.P. Weijland. *Process Algebra*. Cambridge Tracts in Theoretical Computer Science. Cambridge University Press, 1990.
- [CC03] Luís Caires and Luca Cardelli. A spatial logic for concurrency (part I). *Inf. Comput.*, 186(2):194–235, 2003.
- [CG00] Luca Cardelli and Andrew D. Gordon. Anytime, anywhere: Modal logics for mobile ambients. In Mark N. Wegman and Thomas W. Reps, editors, *POPL 2000, Proceedings of the 27th ACM SIGPLAN-SIGACT Symposium on Principles of Programming Languages, Boston, Massachusetts, USA, January 19-21, 2000*, pages 365–377. ACM, 2000.
- [CGG⁺18] Vincenzo Ciancia, Stephen Gilmore, Gianluca Grilletti, Diego Latella, Michele Loretì, and Mieke Massink. Spatio-temporal model checking of vehicular movement in public transport systems. *Int. J. Softw. Tools Technol. Transf.*, 20(3):289–311, 2018.
- [CGL⁺23a] Vincenzo Ciancia, David Gabelaia, Diego Latella, Mieke Massink, and Erik P. de Vink. On bisimilarity for polyhedral models and SLCS. In Marieke Huisman and António Ravara, editors, *Formal Techniques for Distributed Objects, Components, and Systems - 43rd IFIP WG 6.1*

- International Conference, FORTE 2023, Lisbon, Portugal, June 19-23, 2023, Proceedings*, volume 13910 of *Lecture Notes in Computer Science*, pages 132–151. Springer, 2023.
- [CGL⁺23b] Vincenzo Ciancia, Jan Friso Groote, Diego Latella, Mieke Massink, and Erik P. de Vink. Minimisation of spatial models using branching bisimilarity. In Marsha Chechik, Joost-Pieter Katoen, and Martin Leucker, editors, *Formal Methods - 25th International Symposium, FM 2023, Lübeck, Germany, March 6-10, 2023, Proceedings*, volume 14000 of *Lecture Notes in Computer Science*, pages 263–281. Springer, 2023.
- [CLLM14] Vincenzo Ciancia, Diego Latella, Michele Loreti, and Mieke Massink. Specifying and verifying properties of space. In Josep Díaz, Ivan Lanese, and Davide Sangiorgi, editors, *Theoretical Computer Science - 8th IFIP TC 1/WG 2.2 International Conference, TCS 2014, Rome, Italy, September 1-3, 2014. Proceedings*, volume 8705 of *Lecture Notes in Computer Science*, pages 222–235. Springer, 2014.
- [CLLM16] Vincenzo Ciancia, Diego Latella, Michele Loreti, and Mieke Massink. Model checking spatial logics for closure spaces. *Logical Methods in Computer Science*, 12(4), 2016.
- [CLM⁺16] Vincenzo Ciancia, Diego Latella, Mieke Massink, Rytis Paskauskas, and Andrea Vandin. A tool-chain for statistical spatio-temporal model checking of bike sharing systems. In Tiziana Margaria and Bernhard Steffen, editors, *Leveraging Applications of Formal Methods, Verification and Validation: Foundational Techniques - 7th International Symposium, ISoLA 2016, Imperial, Corfu, Greece, October 10-14, 2016, Proceedings, Part I*, volume 9952 of *Lecture Notes in Computer Science*, pages 657–673, 2016.
- [CLM19] Vincenzo Ciancia, Diego Latella, and Mieke Massink. Embedding RCC8D in the collective spatial logic CSLCS. In Michele Boreale, Flavio Corradini, Michele Loreti, and Rosario Pugliese, editors, *Models, Languages, and Tools for Concurrent and Distributed Programming - Essays Dedicated to Rocco De Nicola on the Occasion of His 65th Birthday*, volume 11665 of *Lecture Notes in Computer Science*, pages 260–277. Springer, 2019.
- [CLM25] Vincenzo Ciancia, Diego Latella, and Mieke Massink. Ten years of spatial model checking. In Edward A. Lee, Mohammad Reza Mousavi, and Carolyn L. Talcott, editors, *Rebeca for Actor Analysis in Action - Essays Dedicated to Marjan Sirjani on the Occasion of Her 60th Birthday*, Lecture Notes in Computer Science, pages 406–424. Springer, 2025.
- [CLMV22] Vincenzo Ciancia, Diego Latella, Mieke Massink, and Erik P. de Vink. Back-and-Forth in Space: On Logics and Bisimilarity in Closure Spaces. In N. Jansen, M. Stoelinga, and P. van den Bos, editors, *A Journey From Process Algebra via Timed Automata to Model Learning - Essays Dedicated to Frits Vaandrager on the Occasion of His 60th Birthday*, volume 13560 of *Lecture Notes in Computer Science*, pages 98–115. Springer, 2022.
- [CLMV25] Vincenzo Ciancia, Diego Latella, Mieke Massink, and Erik P. de Vink. On bisimilarity for quasi-discrete closure spaces. *Logical Methods in Computer Science*, Volume 21, Issue 3, Aug 2025.
- [CM26] Vincenzo Ciancia and Mieke Massink. Artefact including the reproducible experimental evaluation of the **VoxMinX** toolchain. Zenodo, 2026.
- [CR08] Anthony G. Cohn and Jochen Renz. Qualitative spatial representation and reasoning. In Frank van Harmelen, Vladimir Lifschitz, and Bruce W. Porter, editors, *Handbook of Knowledge Representation*, volume 3 of *Foundations of Artificial Intelligence*, pages 551–596. Elsevier, 2008.
- [Gal03] A. Galton. A generalized topological view of motion in discrete space. *Theoretical Computer Science. Elsevier.*, 305((1-3)):111–134, 2003.
- [GJ25] Jan Friso Groote and David N. Jansen. A state-based $O(m \log n)$ partitioning algorithm for branching bisimilarity. In Patricia Bouyer and Jaco van de Pol, editors, *36th International Conference on Concurrency Theory, CONCUR 2025, Aarhus, Denmark, August 26-29, 2025*, volume 348 of *LIPICs*, pages 18:1–18:16. Schloss Dagstuhl - Leibniz-Zentrum für Informatik, 2025.
- [GJKW17] Jan Friso Groote, David N. Jansen, Jeroen J. A. Keiren, and Anton Wijs. An $O(m \log n)$ algorithm for computing stuttering equivalence and branching bisimulation. *ACM Trans. Comput. Log.*, 18(2):13:1–13:34, 2017.
- [GM14] Jan Friso Groote and Mohammad Reza Mousavi. *Modeling and Analysis of Communicating Systems*. MIT Press, 2014.

- [GW96] Rob J. van Glabbeek and W. P. Weijland. Branching time and abstraction in bisimulation semantics. *J. ACM*, 43(3):555–600, 1996.
- [HJK⁺15] Iman Haghghi, Austin Jones, Zhaodan Kong, Ezio Bartocci, Radu Grosu, and Calin Belta. Spatel: a novel spatial-temporal logic and its applications to networked systems. In Antoine Girard and Sriram Sankaranarayanan, editors, *Proceedings of the 18th International Conference on Hybrid Systems: Computation and Control, HSCC'15, Seattle, WA, USA, April 14-16, 2015*, pages 189–198. ACM, 2015.
- [IJK⁺21] Fabian Isensee, Paul F. Jaeger, Simon A. A. Kohl, Jens Petersen, and Klaus H. Maier-Hein. nnU-Net: a self-configuring method for deep learning-based biomedical image segmentation. *Nature Methods*, 18:203–211, 2021.
- [IWU⁺24] Fabian Isensee, Tassilo Wald, Constantin Ulrich, Michael Baumgartner, Saikat Roy, Klaus H. Maier-Hein, and Paul F. Jäger. nnU-Net revisited: A call for rigorous validation in 3d medical image segmentation. In Marius George Linguraru, Qi Dou, Aasa Feragen, Stamatia Giannarou, Ben Glocker, Karim Lekadir, and Julia A. Schnabel, editors, *Medical Image Computing and Computer Assisted Intervention - MICCAI 2024 - 27th International Conference, Marrakesh, Morocco, October 6-10, 2024, Proceedings, Part IX*, volume 15009 of *Lecture Notes in Computer Science*, pages 488–498. Springer, 2024.
- [JGKW20] David N. Jansen, Jan Friso Groote, Jeroen J.A. Keiren, and Anton Wijs. An $O(m \log n)$ algorithm for branching bisimilarity on labelled transition systems. In Armin Biere and David Parker, editors, *Tools and Algorithms for the Construction and Analysis of Systems - 26th International Conference, TACAS 2020, Proceedings, Part II*, volume 12079 of *Lecture Notes in Computer Science*, pages 3–20. Springer, 2020.
- [JK26] Sebastian Junges and Guy Katz, editors. *Faster Signature Refinement for Branching Bisimilarity Minimization*, volume 16505 of *Lecture Notes in Computer Science*. Springer, 2026.
- [LCIB13] Bradley C. Lowekamp, David T. Chen, Luis Ibáñez, and Daniel J. Blezek. The design of simpleitk. *Frontiers Neuroinformatics*, 7:45, 2013.
- [LPS20] Sven Linker, Fabio Papacchini, and Michele Sevegnani. Analysing spatial properties on neighbourhood spaces. In Javier Esparza and Daniel Král', editors, *45th International Symposium on Mathematical Foundations of Computer Science, MFCS 2020, August 24-28, 2020, Prague, Czech Republic*, volume 170 of *LIPICs*, pages 66:1–66:14. Schloss Dagstuhl - Leibniz-Zentrum für Informatik, 2020.
- [LQ23] Michele Loreti and Michela Quadrini. A spatial logic for simplicial models. *Log. Methods Comput. Sci.*, 19(3), 2023.
- [Mil09] Robin Milner. *The Space and Motion of Communicating Agents*. Cambridge University Press, 2009.
- [MLI⁺14] Matthew M. McCormick, Xiaoxiao Liu, Luis Ibanez, Julien Jomier, and Charles Marion. ITK: enabling reproducible research and open science. *Frontiers in Neuroinformatics*, 8, 2014.
- [NBC⁺18] Laura Nenzi, Luca Bortolussi, Vincenzo Ciancia, Michele Loreti, and Mieke Massink. Qualitative and quantitative monitoring of spatio-temporal properties with SSTL. *Logical Methods in Computer Science*, 14(4), 2018.
- [Str25] Antonio Strippoli. VoxLogicA UI: Supporting declarative medical image analysis, 2025.
- [SW07] Michael B. Smyth and Julian Webster. Discrete spatial models. In Marco Aiello, Ian Pratt-Hartmann, and Johan van Benthem, editors, *Handbook of Spatial Logics*, pages 713–798. Springer, 2007.
- [TPGN15] Christos Tsigkanos, Liliana Pasquale, Carlo Ghezzi, and Bashar Nuseibeh. Ariadne: Topology aware adaptive security for cyber-physical systems. In Antonia Bertolino, Gerardo Canfora, and Sebastian G. Elbaum, editors, *37th IEEE/ACM International Conference on Software Engineering, ICSE 2015, Florence, Italy, May 16-24, 2015, Volume 2*, pages 729–732. IEEE Computer Society, 2015.
- [Č66] Eduard Čech. Topological Spaces. In Vlastimil Pták, editor, *Topological Spaces*, chapter III, pages 233–394. Publishing House of the Czechoslovak Academy of Sciences/Interscience Publishers, John Wiley & Sons, Prague/London-New York-Sydney, 1966. Revised edition by Zdeněk Frolic and Miroslav Katětov. Scientific editor, Vlastimil Pták. Editor of the English translation, Charles O. Junge. MR0211373.

- [Zev22] Floris Zeven. Spatial model checking with mCRL2. Master's thesis, Eindhoven University of Technology, 2022.

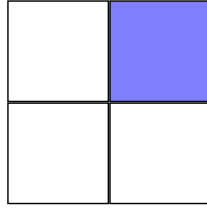


FIGURE 18. Running example: 4 pixels, 1 blue and 3 white

APPENDIX A. RUNNING EXAMPLE FOR *VoxMinX*

To illustrate the various intermediate steps of the *VoxMin* toolchain in Figure 12 and the file formats that are involved, we show the toolchain at work on a micro example of an image of 2 by 2 pixels, composed of three white pixels and one blue, as shown in Figure 18.

1) Encoding phase. The encoding (Box 3 in Figure 12) of the image in Figure 18 is produced with the `convert`-option of *GraphLogicA* that implements the encoding procedure of Section 4.2. The resulting LTS (in the `aut` format accepted by *mCRL2*) is the following:

```
des (0,16,4)
(0, cFFFFFF,0)
(0,change,1)
(0,tau,2)
(0,tau,3)
(1, c3F51B5,1)
(1,change,0)
(1,change,2)
(1,change,3)
(2, cFFFFFF,2)
(2,tau,0)
(2,change,1)
(2,tau,3)
(3, cFFFFFF,3)
(3,tau,0)
(3,change,1)
(3,tau,2)
```

This format reads as follows. The first line is a descriptor stating that the LTS has initial state 0, and it is composed of 16 transitions and 4 states. In the next 16 lines the transitions are listed as triples composed of the source state, the label and the target state. The labels are either `tau` or `change`, or one of the two colours in the image, `cFFFFFF` (denoting white) and `c3F51B5` (denoting the particular shade of blue). Let's call this file `pm_1b3w.aut`.

GraphLogicA also produces a frame file from the images if the `-framefile` option is added. This file, `pm_1b3w.mcrl`, is generated in the *mCRL2* model specification format:

```
act
```

```
cFFFFFFF,
c3F51B5,
change;
init delta;
```

The only purpose of this mCRL2 file is to define the three action labels, cFFFFFFF, c3F51B5 and change (the tau-action is assumed to be present by default). The frame file does not specify any behaviour (as denoted by the delta process that stands for inaction).

2) Conversion of the aut file and frame file to the internal lts format. In VoxMinX the frame file pm_1b3w.mcr1, together with the file pm_1b3w.aut, are converted into an LTS in the lts format of mCRL2 using the ltsconvert function with the -l option (see Box 4 in Figure 12).

3) LTS minimisation. The pm_1b3w.lts file, produced in the previous step, is minimised using the ltsconvert -add-state-as-state-label -branching-bisim operation (also this occurs in Box 4 in Figure 12). This results in a minimised LTS in lts format (pm_1b3w.min.lts). From the latter, information on the relationship between the states in the full LTS and the minimised LTS can be obtained using the ltsinfo operator (see Box 9 in Figure 12) on the minimal LTS resulting in the following file:

```
Number of states: 2.
Number of action labels: 4 (including a tau label).
Number of transitions: 4.
Number of state labels: 2.
LTS is deterministic.
This lts has no probabilistic states.
The state labels of this labelled transition system:
0: (1).
1: (3).
1: (2).
1: (0).
```

The above file shows that the minimised LTS has 2 states: state 0 and state 1. These represent the two equivalence classes. The last four lines report how the states of the minimised LTS (states 0 and 1) are related to the original states of the encoded LTS (0, 1, 2, 3). In particular it says that state 1 of the original model in pm_1b3w.aut is mapped to equivalence class 0 and the other three states (0, 2 and 3, between brackets) are mapped to the equivalence class 1. Note that state 1 in the encoded LTS in pm_1b3w.aut has indeed a transition (self-loop) labeled with c3F51B5, i.e. denoting blue, and states 0, 2 and 3 have self-loops with label cFFFFFFF, i.e. denoting white.

4) Producing a graph model for model checking with GraphLogicA. The minimal LTS, in turn, is translated back (see Box 5 in Figure 12), first into the aut format, using the mCRL2 operation ltsconvert -enone -in=lts pm_1b3w.min.lts -out=aut pm_1b3w.min.aut, resulting in the following file:

```
des (1,4,2)
(1,"change",0)
(1,"cFFFFFFF",1)
(0,"c3F51B5",0)
```

```
(0,"change",1)
```

Next, this aut file is transformed into a json file, representing a finite closure model, accepted by the model checker `GraphLogicA` shown below:

```
{
  "nodes": [
    {
      "id": "1",
      "atoms": [
        "cFFFFFF"
      ]
    },
    {
      "id": "0",
      "atoms": [
        "c3F51B5"
      ]
    }
  ],
  "arcs": [
    {
      "source": "1",
      "target": "0"
    },
    {
      "source": "0",
      "target": "1"
    }
  ]
}
```

The above transformation is provided by the `GraphLogicA` tool itself, using the following command `GraphLogicA -convert pm_1b3w.min.aut pm_1b3w.min.json`. The latter json file is used by `GraphLogicA` for spatial model checking on the closure model. In particular, this file is called from within the logical specification file given as input to `GraphLogicA`. An example is shown below.

```
load graph = "pm_1b3w.min.json"

let white = ap("cFFFFFF")
let blue = ap("c3F51B5")

// wtchb: property "white pixels that are touching blue", defined below
let wtchb = white & touch(white,blue)

save "white.json" white
save "blue.json" blue

save "wtchb.json" wtchb
```

The first line loads the minimised model as a closure model with points in the model representing the equivalence classes. It then defines two atomic propositions, one for the white point (“node” with id=1) and one for the blue point (“node” with id=0) in the model, and a simple property for white points touching the blue one. Finally, three results are saved (in json format). The model checking result `wtchb.json`, for the white points touching blue ones, is as follows.

```
{
  "nodes": [
    {
      "id": "1",
      "atoms": [
        "result",
        "cFFFFFF"
      ]
    },
    {
      "id": "0",
      "atoms": [
        "c3F51B5"
      ]
    }
  ],
  "arcs": [
    {
      "source": "1",
      "target": "0"
    },
    {
      "source": "0",
      "target": "1"
    }
  ]
}
```

Note that this result file looks very similar to the json model file that `GraphLogicA` takes as input, but now the points (i.e. equivalence classes) that satisfy the property (`wtchb` in this case) have an additional label, `result`. In the above file the node with label `"cFFFFFF"` has this additional label.

5) Translating the result back to the original images. Finally, we convert the decorated graph model in json format back into an `aut` file using `GraphLogicA` and the `convert` option. We then extract, via the Python script `resultaut2rts.py`, from the `aut` file an `rts` file that lists all the nodes of the minimal model that satisfy the property `wtchb`. There is only one such class, and this is class 1.

```
[
  1
]
```

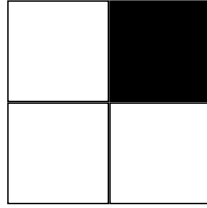


FIGURE 19. Running example model checking result for atomic proposition `white`: 4 pixels, 1 black and 3 white.

This result can be projected (see Box 11 in Figure 12) onto the original image via another Python script `glresults.py` that takes as input the original image, the `pm_1b3w.min.info` file and the `wtchb.rts` file. The resulting image has four pixels, the three white ones where the property `wtchb` holds, and one black one denoting that property `wtchb` does not hold in the blue pixel. The result is shown in Figure 19.

The procedure involves various file transformations and the writing and reading of intermediate files. This is because the current toolchain is a prototype and allowing to study the time each intermediate step takes. In future work we plan to integrate the various steps of the procedure keeping intermediate results in appropriate data structures avoiding time and memory lost in I/O.